Doctoral Thesis

Non-equilibrium stochastic thermodynamics of Brownian particle in an active bath

Jin Tae Park

Department of Physics

Ulsan National Institute of Science and Technology

2021

Non-equilibrium stochastic thermodynamics of Brownian particle in an active bath

Jin Tae Park

Department of Physics

Ulsan National Institute of Science and Technology

Non-equilibrium stochastic thermodynamics of Brownian particle in an active bath

A thesis/dissertation submitted to UNIST
in partial fulfillment of the
requirements for the degree of
Doctor of Philosophy

Jin Tae Park

12 / 17 / 2020
Approved by

_____

Advisor
Hyuk Kyu Pak

Non-equilibrium stochastic thermodynamics of Brownian particle in an active bath

Jin Tae Park

This certifies that the thesis/dissertation of Jin Tae Park is approved.

12 / 17 / 2020

Signature

_____

Advisor: Hyuk Kyu Pak

Signature

_____

Steve Granick

Signature

_____

Yoon-Kyoung Cho

Signature

_____

Joonwoo Jeong

Signature

_____

Chulan Kwon

Abstract

Particles kicked by external forces to produce mobility distinct from thermal diffusion are an iconic feature of the active matter problem. One example is the passive particles in the bath of active particles, such as swimming bacteria. In this case, the fluctuation of the particle position is influenced by the thermal and the active fluctuations simultaneously. Here, we map this onto a minimal model for experiment and theory covering the wide time and length scales of usual active matter systems. A particle`s diffusion perturbed by a programmable harmonic potential (optical trap) is captured. It gives a time correlated active kicks with a random interval following the Poisson process. The model's generic simplicity allows us to find conditions for which displacements are Gaussian (or not), how diffusion is perturbed (or not) by kicks, and quantifying heat dissipation to maintain the non-equilibrium steady state in an active bath. The model proposed in the work successful reproduces the experimental results, as shown on example of the tracer mobility in an active bath of swimming algal cells. It can be used as a stochastic dynamic simulator for Brownian objects in various active baths without mechanistic understanding, owing to the generic framework of the protocol.

Contents

List of Figures

I Introduction

1.1 Background

Nature is surrounded by numerous active matters. These active particles move either by using an internal energy source or by receiving energy from the outside. In addition, they sometimes transmit energy to the passive Brownian particles nearby by collisions and in this way boost their mobility. In these cases, the Brown particle acts as a good tracer particle that can investigate the surrounding active matters. A lot of researches have been done to understand the key problems that arise from swimming bacteria[1-8], active colloids[9-11], enzyme reactions [12-14] , and even chemical reation.[15] In this thesis, we are not interested in the different features of these systems. One of the important common features is long-range interaction (usually hydrodynamic), which is difficult to implement experimentally or theoretically. Along with the complexity of this active environment[4, 16, 17], it is difficult to define and control the various parameters that represent these systems. For example, in the case of bacteria, it is impossible to control the activity, their concentration, and the number of collisions with surrounding passive particles. As a result, some bacterial experiments show that the probability distribution function (PDF) is Gaussian, but others show non-Gaussian. Besides, the energy flowing into passive particles from swimming bacteria is unclear[18]. Without a detailed understanding of the active system, we would like to use a simple model that can explain experimentally and theoretically when the PDF shows non-Gaussian or Gaussian diffusion and how energy flows. Here, we only deal with a strongly-overdamped system - life at low Reynolds numbers.[19, 20]

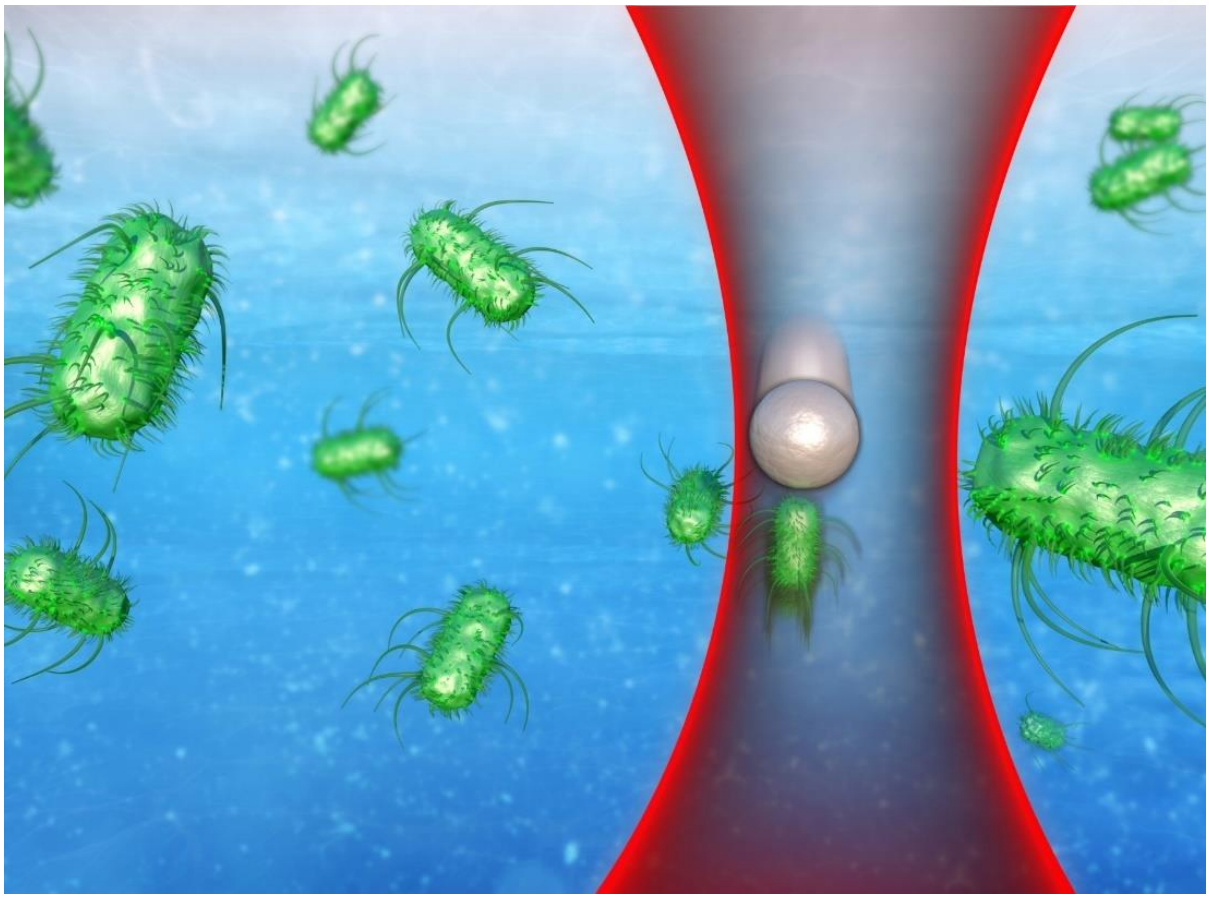

Figure 1: Artistic view of the model. A tracer particle trapped in an optical harmonic potential is surrounded by active partlces such as bacteria.

1.2 Active force modelling

To mimic a tracer particle surrounded by a real active matter system in a thermal environment,[21, 22] we use an optical trapping[23] force that changes over time. The tracer particle is surrounded by a viscous medium, feels the time-dependent harmonic potential from the optical trapping. We assume that an active force is generated by time-dependent optical random kicks, which represent the interaction force between the active particles and the tracer particle. Each kick affects the tracer particle in time and decays quickly. Figure 2 shows how to generate the active force which is created by shifting the center position of the optical potential for a programmed duration time. Since the diffusion process of the tracer particle releases energy into the thermal bath, immediately after the kicking the system starts relaxing to equilibrium until the next kick occurs.

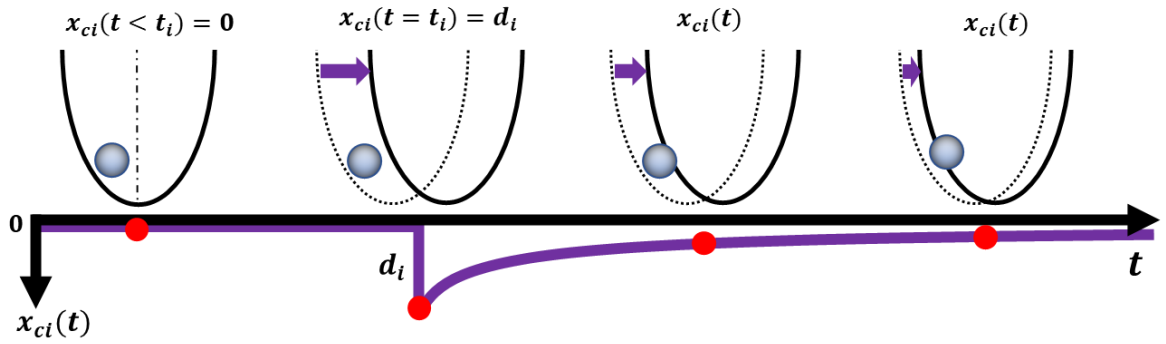

Figure 2: How to generate the active force in time.

In this work, we study only one-dimensional dynamics of the tracer particle in a harmonic potential for simplicity. The tracer particle is also influenced by thermal noise $\xi_{th}(t)$ from the surrounding media and by fluctuating active force $\xi_{act}(t)$ from the random kicks. Therefore, the motion of the tracer particle is described as

$$\gamma\dot{x} = -kx(t) + \xi_{th}(t) + \xi_{act}(t) = -kx(t) + \xi_{th}(t) + kx_c(t). \quad (1)$$

Here, k is the harmonic potential stiffness and γ is the coefficient of dissipation that is representing the viscosity of solvent. The thermal noise is Gaussian white noise without memory. Without the active force $\xi_{act}(t)$, Eq.(1) is a well-known simple Langevin equation which describes how a Brownian particle moves within the harmonic potential. This system has a characteristic time constant $\tau_k \equiv \gamma/k$, which is the time to reach equilibrium when the particle is within the harmonic potential.

In our model, the active force acting on the tracer particle is determined by three parameters: the average time interval between kicks τ_p, kick duration τ_c, and random kick amplitude X. (Fig. 3).

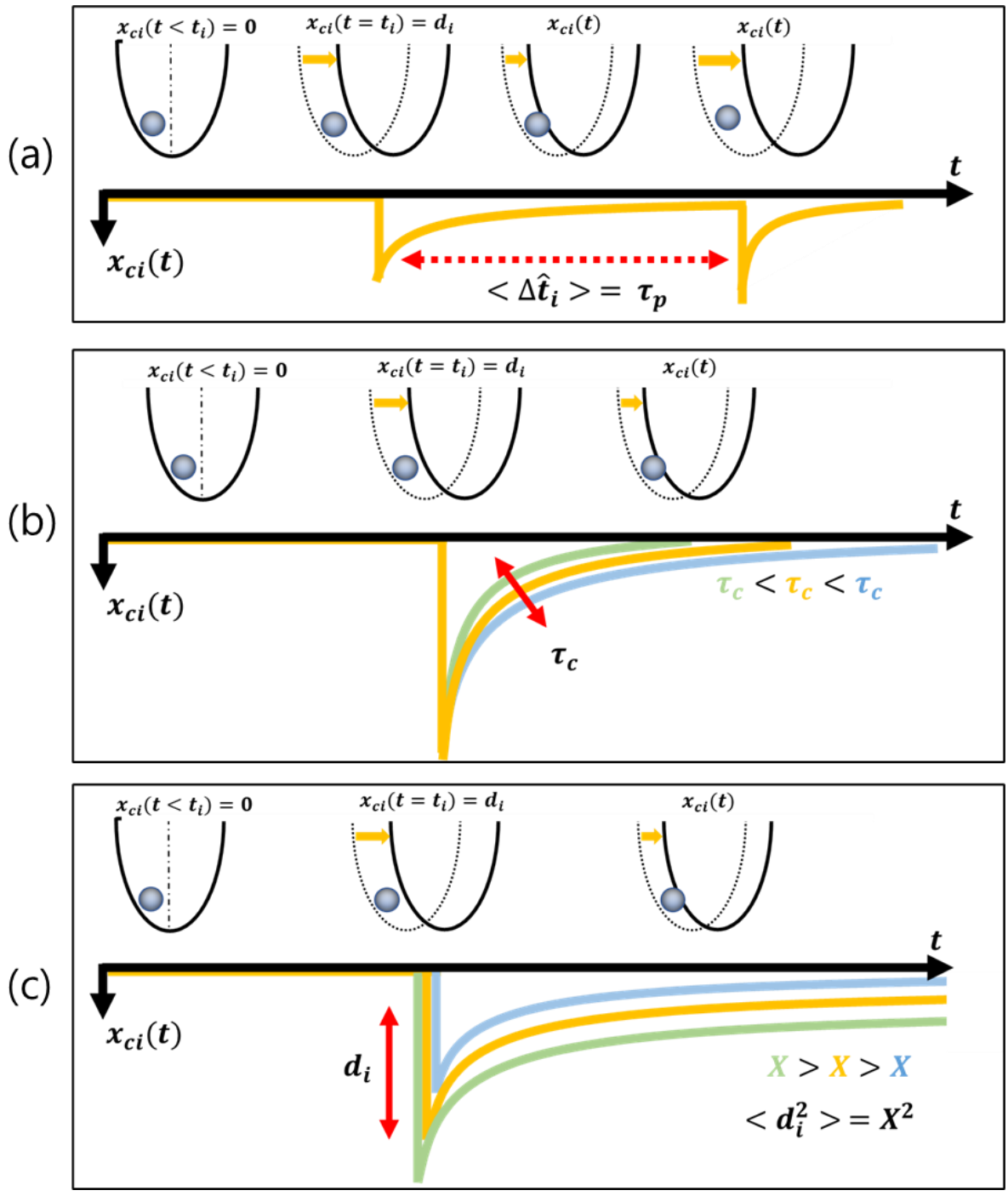

Figure 3: Graphical description of three control parameters: (a) random Poisson interval time τ_p, (b) kick duration time τ_c, and (c) kick strength X.

Each parameter represents a certain characteristic property of the actual active force. The average Poisson time τ_p represents the average interval between successive kicks (see Fig.3 (a)). The interaction between the tracer particle and the active particles is not continuous in time. Instead, it occurs randomly and discontinuously. The larger the concentration of the active particles, the more frequent random kicks for a given time. The Poisson interval τ_p is related to the concentration of active particles[24, 25]. The kick duration time τ_c represents the correlation time of the interaction. It is related to the characteristic persistence time of the active particle. Thus, for each collision, the active particle exerts a force on the tracer particle for the average duration τ_c, as shown in Fig.3 (b). The last parameter is the root-mean-square value of the random kick amplitude X, which is related to the average strength of the kick (Fig.3 (c)). Since the tracer particle is surrounded by active particles, the kick strength follows a Gaussian distribution with zero mean and variance X^2. The larger mobility of the active particle, the larger kicking force, and so is the magnitude of X.

The active force with three control parameters is designed as follows. The time interval between successive kicks is t_i which satisfies the Poisson random process. Each kick arriving at the time t_i instantaneously shifts the trap center by x_{ci} which has a random amplitude d_i with variance X^2 and decays exponentially with the time constant τ_c, as illustrated in Fig. 3. Therefore, the position of the trap center $x_c(t)$ at a given time is expressed as the sum of all the previous kicks,

$$x_c(t) = \sum_i d_i \mathrm{e}^{\frac{-(t-t_i)}{\tau_c}} \theta(t-t_i). \tag{2}$$

Since the active force $\xi_{act}(t) = kx_c(t)$, the time correlation of active force in steady-state is expressed as $\langle \xi_{act}(t)\xi_{act}(s)\rangle = (k^2X^2\tau_c/2\tau_p)\mathrm{e}^{-|t-s|/\tau_c}$ which is derived in Section 3.1. Therefore, using the Poisson property of active force and Eq. (2), the Langevin equation of the active force can be expressed as

$$\dot{\xi}_{act}(t) = -\frac{\xi_{act}(t)}{\tau_c} + k\sum_{i=1}^{n} d_i\delta(t-t_i). \tag{3}$$

Here, the Poisson noise is generated by the hidden discrete pulse noise. This equation looks very similar to the well-known Ornstein-Uhlenbeck (OU) noise. The OU noise is expressed as $\dot{\xi}_{ou} = -\xi_{ou}/\tau_c + \eta_w(t)$ with the time correlation of $\langle \xi_{ou}(t)\xi_{ou}(s)\rangle \propto \mathrm{e}^{-|t-s|/\tau_c}$.[26] Here, η_w is white Gaussian noise. When comparing the ξ_{act} and ξ_{ou}, both satisfy the exponential correlation, but the additional noise term over time is discontinuous in the former case and continuous in the latter case. The active force model is made with discontinuous characteristics, but when it goes to a limit condition, it becomes the OU noise. In order words, this model can theoretically

explain not only Poisson correlated noise, but also Gaussian correlated noise and even white noise as shown in Figs. 4-6.

When the kick duration time is shorter than the Poisson interval time $\tau_c < \tau_p$, the PDF of the active force shows non-Gaussian distribution as shown in Fig. 4 (b). When the kick duration time is much larger than the Poisson interval time $\tau_c / \tau_p \to \infty$, however, the active force model becomes a Gaussian continuous correlated noise, which is the same as the OU noise model (Fig. 5).[27] The white Gaussian noise is also satisfied when the kick duration time is very short (the limit $\tau_c \to 0$) and the condition of $\tau_p \to \tau_c^2$ is satisfied as shown in Fig. 6.[28] The rigorous proof of the generality of our active force model is shown in Section 3.1.

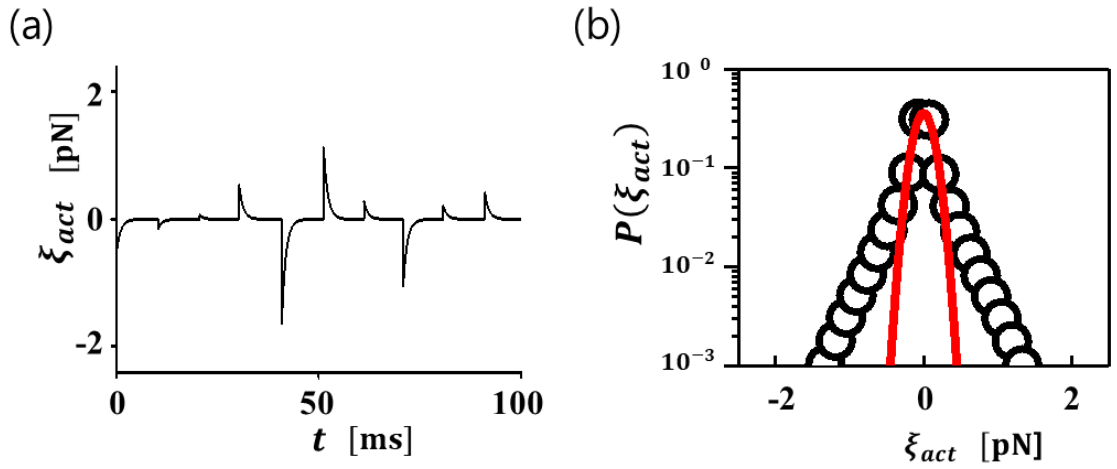

Figure 4: Poisson correlated active force in the case of $\tau_c < \tau_p$. (a) shows active force in time, (b) represents distribution of active force. Here, the red curve is a Gaussian fit.

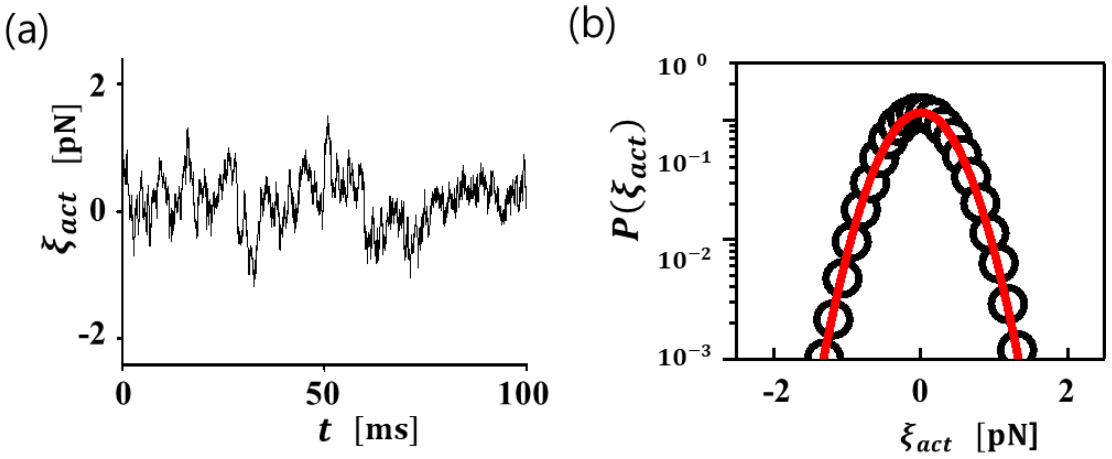

Figure 5: In the limit of $\tau_c/\tau_p \to \infty$, the active force becomes Ornstein-Uhlenbeck noise (a) shows active force in time, (b) represents distribution of active force. Here, the red curve is a Gaussian fit.

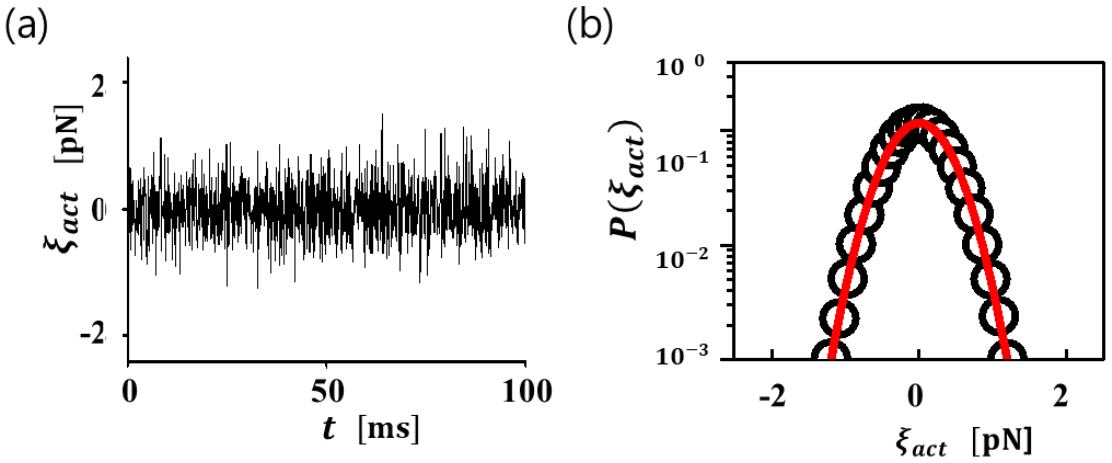

Figure 6: In the limit of $\tau_c \to 0 \,\&\, \tau_p \to \tau_c^2$, the active force becomes white Gaussian noise (a) shows active force in time, (b) represents distribution of active force. Here, the red curve is a Gaussian fit.

II Method

2.1 Single-laser method

Figure 7 shows the instrument layout of the experimental setup, in which trapping and tracking the tracer particle are done simultaneously using a single laser. This is suitable for observing only a single tracer particle, for example, when it is necessary to study the environment in which the particle is surrounded by active matters, or when the tracer particle itself is an active particle. The advantage of this is that the experiment can be performed at a low cost, and the motion of particles can be observed over a very short time range using a quadrant photodetector. The experiments shown in this thesis used the two-laser method, and the single laser method and fluorescence image were designed for future experiments.

2.2 Design of the single-laser method with fluorescence system

We use an acousto-optics modulator (AOD, AA Opto Electronic) to modulate a 1064 nm laser (IPG Photonics) for trapping and a microscope (Olympus, IX73) objective lens (Obj., Olympus 100x, Oil, Numerical aperture: 1.4) to focus the laser beam. The trapping laser power is controlled by the combination of a half-wave plate (Thorlabs, WPH10M-1064) and Glan-Taylor polarizer (Thorlabs, GT10-C). We use the special microscope condenser lens (Con., Olympus, Oil, NA: 1.4) of high numerical aperture. A quadrant photodiode detector (QPD, First sensor) is used to measure the particle position. The fluorescence image system with two excitation lasers (Coherent, OBIS 488 and 532 nm) is not used in this work, but is installed for future purposes. Fluorescence from the sample is passed through an excitation filter F2* (Semrock, FF01-540/50-25 for 488nm, FF01-575/15-25 for 532nm, FF01-890/SP-25 for bright-field image) to remove the excitation lights and excessive optical trapping laser light. The beam of the excitation laser is expanded using the telescope T2 (Thorlabs, GBE10-A) and T3 (Thorlabs, GBE10-A). We align the plane of optical traps by adjusting the position of telescope T1. The camera (EMCCD, Andor) detects the fluorescence signal or take the particles image. The trapping laser light is also used to measure the particle position and is filtered with 1064 nm bandpass filter (F1, Semrock, FF01-1064/5-25) before QPD. The dichroic mirrors are used to combine the optical trapping, fluorescence lasers, and LED (Thorlabs, DC4100) lamp light for illumination. Here, D1 (Semrock, FF509-Di01-25x36), D2 (Semrock, FF749-SDi01-25x36x3.0), D3 (Semrock, FF749-SDi01-25x36x3.0), and D4* (Semrock, Di02-R488-25x36 for 488nm, Di02-R532-25x36 for 532nm laser).

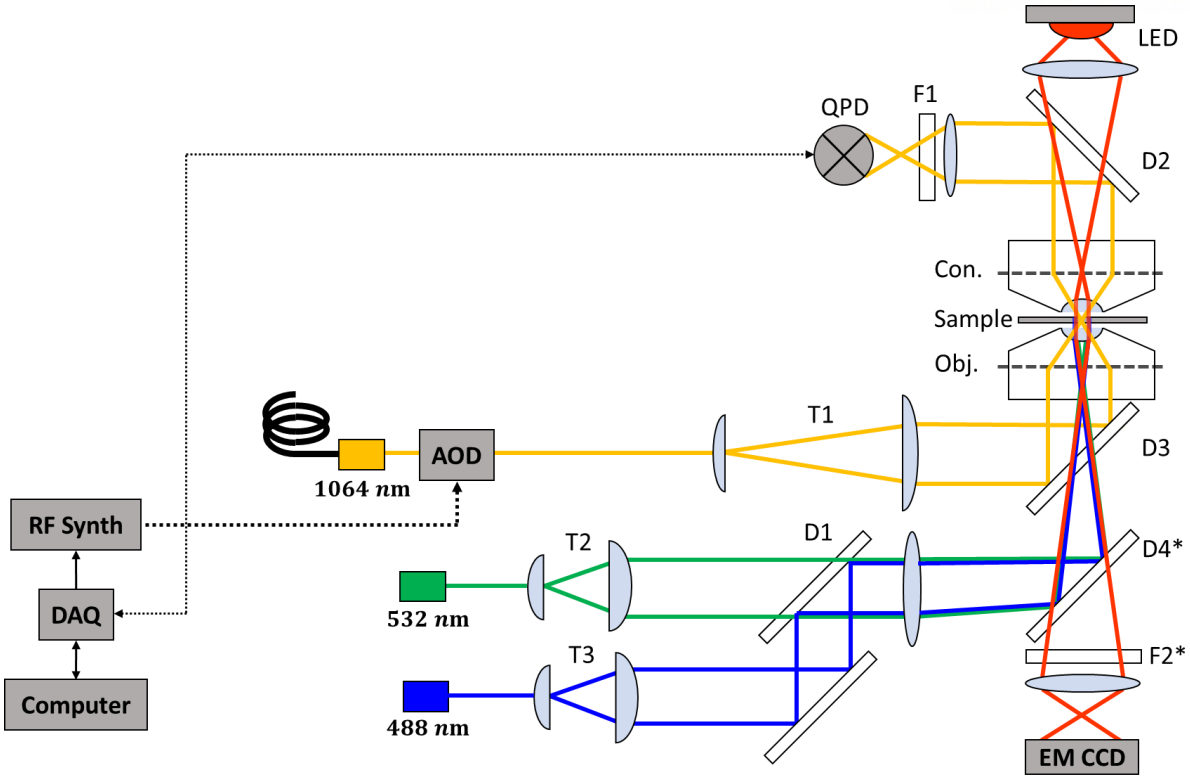

Figure 7: Schematic of experimental setup for fluorescence image with optical trapping. D1-D4, dichroic mirrors; T1-T3, telescopes; F1-F2, filters.

2.3 Two-Laser method

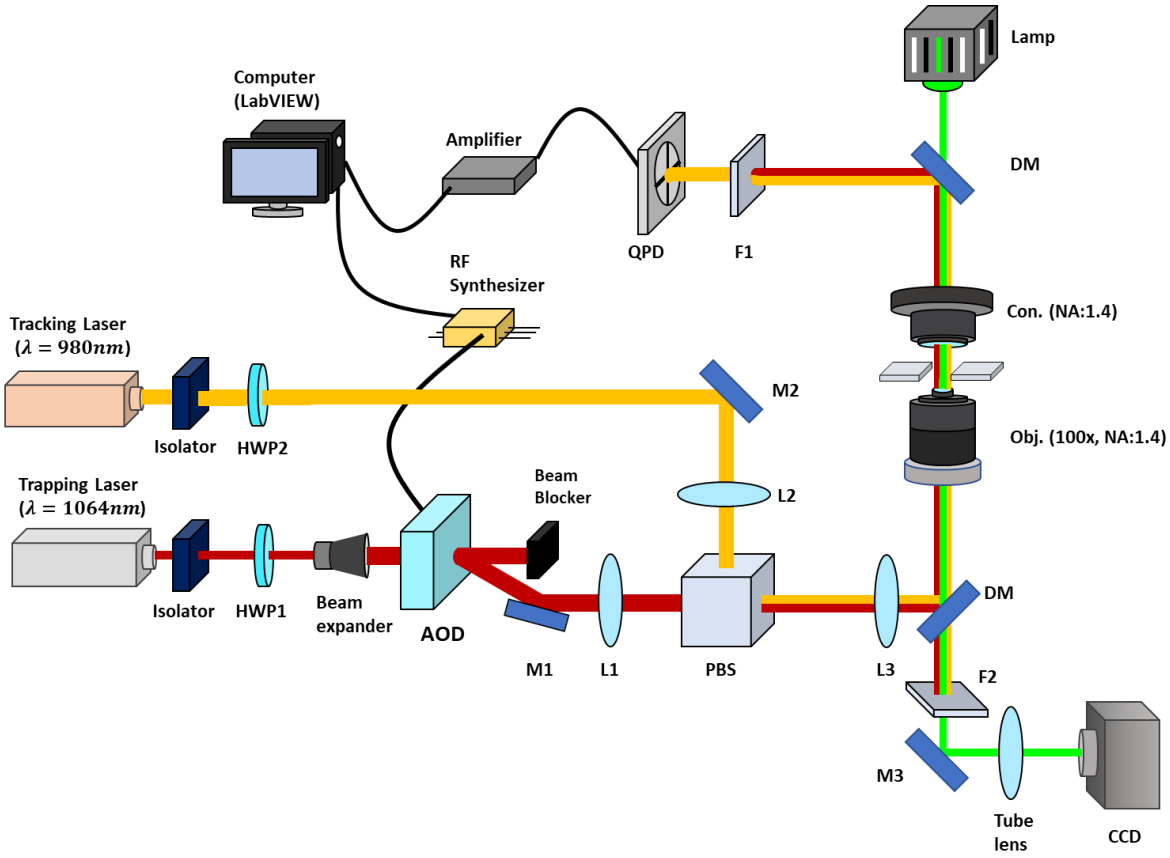

Figure 8: Schematic of the two-laser system for trapping experiment. Here, L1-L3, lens; HWP1-HWP2, half wave plates; F1-F2, filters; M1-M3, mirrors, DM; dichroic mirrors.

In this scheme, two lasers are used[29, 30]: the first laser (1064 nm) to trap the particle, and the second laser (980nm) to track the position of the particle as shown in Fig. 8. Since the tracking laser should not affect the potential of the particle, the tracking laser power should be much lower than trapping laser power. The average power we used in the experiment is $10\sim 20mW$ for trapping laser and $50\mu W$ for tracking laser. The advantage of the two-laser method is that we can vary the center position of the trapping beam over a large distance with time. In the experiment, the position of the 1064 nm laser beam is controlled through LabView using the 1^{st} order beam among the beams passing through the AOD. The AOD and QPD should be placed in the back focal plane position of the objective lens and condense lens to maintain the stiffness of the harmonic potential k when the center position of the trapping beam shifts with time. To measure the particle position very accurately, QPD needs a high magnification current to voltage amplifier because the intensity of the tracking laser is very low ($\sim 50\mu W$). This system has an accuracy of 1nm in the speed of $0.2ms$.

2.4 Experimental details

Experiments were conducted in deionized water in the sample cell which has a channel height of about 100μm by using the double-side tapes between two slide glasses. The concentration of the tracer particles of 2μm polystyrene is $\phi = 1.0\times10^{-6}$ in volume fraction. The temperature is controlled at 295 ± 0.1K. To achieve a non-equilibrium steady state, the trap center $x_c(t)$ is randomly changed according to Eq. (2) by using the AOD [see Fig. 2]. In this experiment, $k = 15.4\,p\text{N}/\mu\text{m}$ and $\tau_k = \gamma/k \cong 1.1m\text{s}$, where the k is trap stiffness and τ_k is the characteristic relaxation time. In Section 4.4.4, to measure the response function $R(\omega)$ in equilibrium condition, $x_c(t)$ is shifted to 100 nm at $t=0$ and the average particle trajectory in relaxation processes is measured in the thermal equilibrium condition. For $R(\omega)$ in the nonequilibrium steady condition, $\Delta x_c(t)$ is additionally shifted at $t=0$ on top of the thermal condition. The ensemble-averaged trajectories showed that both equilibrium and nonequilibrium conditions have the same form of the response function with exponential relaxation behavior with a given τ_k.

2.5 Computer simulation

To compare with the experimental result, we simulate the active force model using the MATLAB program based on the Langevin equation in Eq. (1). The code is in the appendix in Section 5.1.

III Theoretical Development

3.1 Poisson active force and OU noise

The tracer particle is kicked by a series of active forces, each of which is generated randomly at the time t_i with random amplitude d_i. Each kick shifts the center of the trap decaying exponentially with characteristic time τ_c, which is schematically shown in Fig. 2. Then, the active force acting on the tracer particle at a certain time t is the sum of active forces remaining until the time t, given as

$$\xi_{act}(t) = k\sum_i d_i \mathrm{e}^{-(t-t_i)/\tau_c} \cdot \theta(t-t_i) = kx_c(t), \tag{4}$$

where $\theta(t-t_i)$ is the step function, which equals to 1 for $t > t_i$ and 0 otherwise. d_i is a Gaussian random number with variance X^2 and t_i is produced by the Poisson distribution with mean interval τ_P. The resultant position $x_c(t)$ of the center of the harmonic potential is equal to the sum of the active forces divided by k, given in the above equation.

Since the thermal fluctuation and the active force are uncorrelated, the particle position can be expressed as $x \equiv x_{th} + x_{act}$, where x_{th} is due to the thermal noise and x_{act} due to the active force, respectively. Therefore, Eq. (1) in the text can be expressed as a set of two stochastic differential equations that are completely independent of each other.

$$\gamma \dot{x}_{th} = -kx_{th} + \xi_{th}, \qquad \gamma \dot{x}_{act} = -kx_{act} + \xi_{act} \tag{5}$$

Here, $\xi_{th}(t)$ is a usual thermal noise with zero mean and time-correlation $\langle \xi_{th}(t)\xi_{th}(t') \rangle = 2\gamma k_B T \delta(t-t')$ and $\xi_{act}(t)$ is an active force in Eq. (4). The time-correlation function of active forces (for detailed calculation see Section 5.2) is useful to investigate the stochastic properties of the system such as $\langle x^2 \rangle$, $\langle x(t)x(t') \rangle$ etc., where $\langle \cdots \rangle$ denotes the ensemble average over thermal and active forces. We find for $t' > t$

$$\begin{aligned} \langle \xi_{act}(t)\xi_{act}(t') \rangle &= k^2 X^2 \mathrm{e}^{-(t'-t)/\tau_c} \left\langle \sum_i \mathrm{e}^{-2(t-t_i)/\tau_c} \right\rangle \\ &= k^2 X^2 \frac{\tau_c}{2\tau_p} \mathrm{e}^{-(t'-t)/\tau_c} \left(1 - \mathrm{e}^{-2t/\tau_c}\right) \end{aligned} \tag{6}$$

where we use $\langle d_i d_j \rangle = X^2 \delta_{ij}$. Using the property of the Poisson distribution

$$\left\langle \sum_i \mathrm{e}^{-2(t-t_i)/\tau_c} \right\rangle = \int_0^t \frac{ds}{\tau_p} \mathrm{e}^{-2(t-s)/\tau_c}. \tag{7}$$

Using Eq. (7) for steady-state condition ($t >> \tau_c$), the active force autocorrelation function in Eq. (6) takes the following form

$$\left\langle \xi_{act}(t)\xi_{act}(t')\right\rangle = k^2 X^2 \frac{\tau_c}{2\tau_P} \mathrm{e}^{-(t'-t)/\tau_c}. \tag{8}$$

The exponential correlation in this equation is similar to that for the OU noise. The PDF of the active forces has non-zero higher-order cumulants for all orders, unlike the OU noise. As τ_c/τ_p increases, the active noise becomes the OU noise, as shown in Fig. 5.

We can prove rigorously that our model satisfies not only Poisson correlated noise but also OU noise. Integrating Eq. (3) from t to $t+dt$, $\xi_{act}(t+dt) \equiv \xi$ and $\xi_{act}(t) \equiv \xi'$ are related as $\xi = \xi' - (\xi'/\tau_c)dt + h$, in which $h = kd$ for random amplitude d with probability dt/τ_p and $h = 0$ with probability $1 - dt/\tau_p$. Then, the Kolmogorov forward equation, which describes the probability of a certain state in stochastic process changes over time, for Eq. (3) is written up to the first order in dt as

$$\begin{aligned} P(\xi,t+dt) &= \int d\xi' P(\xi',t)\left[\delta\left(\xi-\xi'+\frac{\xi'}{\tau_c}dt\right)\left(1-\frac{dt}{\tau_p}\right)+\delta\left(\xi-\xi'+\frac{\xi'}{\tau_c}dt-kd\right)\left(\frac{dt}{\tau_p}\right)\right] \\ &= \int d\xi' P(\xi',t)\left[\left[1-\frac{dt}{\tau_c}\frac{\partial}{\partial\xi'}\xi'\right]\delta(\xi-\xi')\left(1-\frac{dt}{\tau_p}\right)+\left[1-\frac{dt}{\tau_c}\frac{\partial}{\partial\xi'}\xi'\right]\delta(\xi-kd-\xi')\left(\frac{dt}{\tau_p}\right)\right] \\ &= P(\xi,t)-\frac{dt}{\tau_p}P(\xi,t)+\frac{dt}{\tau_c}\frac{\partial}{\partial\xi}\xi P(\xi,t)+\frac{dt}{\tau_p}P(\xi-kd,t)+\Theta\left(dt^2\right) \\ &= P(\xi,t)+\frac{dt}{\tau_c}\frac{\partial}{\partial\xi}\xi P(\xi,t)+\frac{dt}{\tau_p}\left[P(\xi-kd,t)-P(\xi,t)\right]. \end{aligned} \tag{9}$$

Here, we use the Taylor expansion up to the first order in dt as

$$\begin{aligned} \delta(\xi-\xi'+cdt) &= \delta(\xi-\xi')-\frac{\partial}{\partial\xi'}\left[cdt\,\delta(\xi-\xi')\right]+\Theta\left(dt^2\right) \\ &= \left[1-\frac{\partial}{\partial\xi'}cdt\right]\delta(\xi-\xi') \end{aligned} \tag{10}$$

and the integration is done over ξ'. Then, Taylor expansion of $P(\xi-kd)$ in powers of d and averaging over d is

$$\begin{aligned} P(\xi-kd,t) &= P(\xi,t)-kd\frac{\partial}{\partial\xi}P(\xi,t)+\frac{k^2d^2}{2!}\frac{\partial^2}{\partial\xi^2}P(\xi,t)+\cdots \\ &\quad+\frac{(-1)^n k^n d^n}{n!}\frac{\partial^n}{\partial\xi^n}P(\xi,t). \end{aligned} \tag{11}$$

From Eqs. (9), (10) and (11), we can get the following relation.

$$\frac{\partial P(\xi,t)}{\partial t} = \frac{1}{\tau_c}\frac{\partial}{\partial \xi}\xi P(\xi,t) + \frac{1}{\tau_p}\sum_{n=1}^{\infty}\frac{(-1)^n k^n C_n}{n!}\frac{\partial^n}{\partial \xi^n}P(\xi,t). \tag{12}$$

Here, the C_n represents $\langle d^n \rangle$, then $C_n = 0$ when n is an odd number, because d is satisfied random Gaussian distribution. Also, by changing the variables as $T \equiv t/\tau_c$ and $X \equiv \xi/\sqrt{\Omega}$ for $\Omega \equiv \tau_c/\tau_p$, we find

$$\begin{aligned}\frac{\partial P(X,T)}{\partial T} &= \frac{\partial}{\partial X}XP(X,T) + \Omega\sum_{n=1}^{\infty}\frac{k^n C_n}{n!\Omega^{n/2}}\frac{\partial^n}{\partial X^n}P(X,T) \\ &= \frac{\partial}{\partial X}XP(X,T) + \sum_{n=1}^{\infty}\frac{k^{2n}C_{2n}\Omega^{1-n}}{(2n)!}\frac{\partial^{2n}}{\partial X^{2n}}P(X,T).\end{aligned} \tag{13}$$

In the limit $\Omega(=\tau_c/\tau_p) \to \infty$, the above equation becomes the Fokker Planck equation for the OU process.

$$\frac{\partial P(X,T)}{\partial T} = \frac{\partial}{\partial X}XP(X,T) + \frac{k^2 C_2}{2}\frac{\partial^2}{\partial X^2}P(X,T). \tag{14}$$

This derivation agrees with Fig. 5.

3.2 Power spectral density of the particle position

The power spectral density of the particle position is calculated from Eq. (1) expressed as

$$\left[\gamma\frac{d}{dt}+k\right]x(t)=\xi_{th}(t)+\xi_{act}(t). \tag{15}$$

We can apply the Fourier transform $x(t)=(1/2\pi)\int_{-\infty}^{\infty}\tilde{x}(\omega)e^{i\omega t}d\omega$ to Eq. (15).

$$\begin{aligned}\Rightarrow&\left[\gamma\frac{d}{dt}+k\right]\frac{1}{2\pi}\int_{-\infty}^{\infty}\tilde{x}(\omega)e^{i\omega t}d\omega=\frac{1}{2\pi}\left[\int_{-\infty}^{\infty}\tilde{\xi}_{th}(\omega)e^{i\omega t}d\omega+\int_{-\infty}^{\infty}\tilde{\xi}_{act}(\omega)e^{i\omega t}d\omega\right]\\ \Rightarrow&\frac{1}{2\pi}\int_{-\infty}^{\infty}\left[\gamma\frac{d}{dt}+k\right]\tilde{x}(\omega)e^{i\omega t}d\omega=\frac{1}{2\pi}\left[\int_{-\infty}^{\infty}\tilde{\xi}_{th}(\omega)e^{i\omega t}d\omega+\int_{-\infty}^{\infty}\tilde{\xi}_{act}(\omega)e^{i\omega t}d\omega\right]\end{aligned} \tag{16}$$

$$\Rightarrow\frac{1}{2\pi}\int_{-\infty}^{\infty}[i\gamma\omega+k]\tilde{x}(\omega)e^{i\omega t}d\omega=\frac{1}{2\pi}\int_{-\infty}^{\infty}\left[\tilde{\xi}_{th}(\omega)+\tilde{\xi}_{act}(\omega)\right]e^{i\omega t}d\omega \tag{17}$$

From Eq. (17), the particle position function $x(\omega)$ is expressed as

$$[i\gamma\omega+k]\tilde{x}(\omega)=\tilde{\xi}_{th}(\omega)+\tilde{\xi}_{act}(\omega) \tag{18}$$

$$\Rightarrow\tilde{x}(\omega)=\frac{\tilde{\xi}_{th}(\omega)+\tilde{\xi}_{act}(\omega)}{i\gamma\omega+k}. \tag{19}$$

Therefore, the power spectral density $S_{xx}(\omega)$ of position can be obtained as follows.

$$S_{xx}(\omega)\equiv\left\langle\left|\tilde{x}(\omega)\right|^2\right\rangle=\frac{\left\langle\left|\tilde{\xi}_{th}(\omega)+\tilde{\xi}_{act}(\omega)\right|^2\right\rangle}{\gamma^2\omega^2+k^2} \tag{20}$$

$$\therefore S_{xx}(\omega)=\frac{2/\tau_k}{\omega^2+(1/\tau_k)^2}\left[\frac{k_BT}{k}+\frac{k_BT_{act}}{k}\cdot\left(1+\frac{\tau_c}{\tau_k}\right)\cdot\frac{1}{1+\omega^2\tau_c^2}\right] \tag{21}$$

Here, $T_{act}\equiv kX^2\tau_c^2/[2k_B\tau_p\tau_k(1+\tau_c/\tau_k)]$ is the active temperature whose physical meaning will be explained in Section 4.1. Experimental data of the power spectral density with active force are shown in Section 4.4.2.

3.3 Autocorrelation function

The autocorrelation function of the particle position can be easily calculated from the power spectral density because it satisfies the Fourier relationship.

$$\left\langle x(t)x(0)\right\rangle = \mathrm{F}^{-1}\left(\left\langle\left|\tilde{x}(\omega)\right|^2\right\rangle\right) = \mathrm{F}^{-1}\left(S_{xx}(\omega)\right) \tag{22}$$

Using Eq. (21), Eq. (22) is expressed as

$$\begin{aligned}
&= \mathrm{F}^{-1}\left(\frac{2/\tau_k}{\omega^2+\left(1/\tau_k\right)^2}\left[\frac{k_BT}{k}+\frac{k_BT_{act}}{k}\cdot\left(1+\frac{\tau_c}{\tau_k}\right)\cdot\frac{1}{1+\omega^2\tau_c^2}\right]\right)\\
&= \frac{k_BT}{k}\mathrm{F}^{-1}\left(\frac{2/\tau_k}{\omega^2+\left(1/\tau_k\right)^2}\right)+\frac{k_BT_{act}}{k}\cdot\left(1+\frac{\tau_c}{\tau_k}\right)\mathrm{F}^{-1}\left(\frac{2/\tau_k}{\omega^2+\left(1/\tau_k\right)^2}\cdot\frac{1}{1+\omega^2\tau_c^2}\right)\\
&= \frac{k_BT}{k}\mathrm{e}^{-\frac{t}{\tau_k}}+\frac{k_BT_{act}}{k}\cdot\left(1+\frac{\tau_c}{\tau_k}\right)\frac{\mathrm{e}^{-\frac{t}{\tau_k}}-\frac{\tau_c}{\tau_k}\mathrm{e}^{-\frac{t}{\tau_c}}}{1-\frac{\tau_c^2}{\tau_k^2}}.
\end{aligned} \tag{23}$$

Therefore, the autocorrelation of the particle position is expressed as

$$\left\langle x(t)x(0)\right\rangle = \frac{k_BT}{k}\mathrm{e}^{-\frac{t}{\tau_k}}+\frac{k_BT_{act}}{k}\cdot\left(1+\frac{\tau_c}{\tau_k}\right)\frac{\mathrm{e}^{-\frac{t}{\tau_k}}-\frac{\tau_c}{\tau_k}\mathrm{e}^{-\frac{t}{\tau_c}}}{1-\frac{\tau_c^2}{\tau_k^2}}. \tag{24}$$

3.4 Mean square displacement

The mean square displacement (MSD) of a particle under active force is expressed as

$$\left\langle \left[x(t_0+t)-x(t_0) \right]^2 \right\rangle = \left\langle x^2(t_0+t) \right\rangle + \left\langle x^2(t_0) \right\rangle - 2\left\langle x(t_0+t)x(t_0) \right\rangle \tag{25}$$

$$x(t) = x_0 e^{-\frac{k}{r}t} + \frac{1}{\gamma}\int_0^t dt' e^{-\frac{k}{\gamma}(t-t')}\left[\xi_{th}(t') + \xi_{act}(t') \right] \tag{26}$$

$$\begin{aligned} \left\langle x(t)^2 \right\rangle = \left\langle x_0^2 \right\rangle e^{-\frac{2k}{\gamma}t} &+ \frac{1}{\gamma^2}\int_0^t dt' e^{-\frac{k}{\gamma}(t-t')}\int_0^t dt'' e^{-\frac{k}{\gamma}(t-t'')}\left\langle \xi_{th}(t')\xi_{th}(t'') \right\rangle \\ &+ \frac{1}{\gamma^2}\int_0^t dt' e^{-\frac{k}{\gamma}(t-t')}\int_0^t dt'' e^{-\frac{k}{\gamma}(t-t'')}\left\langle \xi_{act}(t')\xi_{act}(t'') \right\rangle \end{aligned} \tag{27}$$

The second term about thermal noise on the right in Eq. (27), can be solved as

$$\frac{1}{\gamma^2}\int_0^t dt' e^{-\frac{k}{\gamma}(t-t')}\int_0^t dt'' e^{-\frac{k}{\gamma}(t-t'')}\left\langle \xi_{th}(t')\xi_{th}(t'') \right\rangle = \frac{2\gamma k_B T e^{-2\frac{k}{\gamma}t}}{\gamma^2}\int_0^t dt'\int_0^t dt'' e^{\frac{k}{\gamma}(t'+t'')}\delta(t'-t''). \tag{28}$$

Here, the time correlation function of the thermal noise $\left\langle \xi_{th}(t')\xi_{th}(t'') \right\rangle = 2\gamma k_B T\delta(t'-t'')$ is used. Then, it is easily calculated as

$$\begin{aligned} &= \frac{2\gamma k_B T e^{-2\frac{k}{\gamma}t}}{\gamma^2}\int_0^t dt'\int_0^t dt'' e^{\frac{k}{\gamma}(t'+t'')}\delta(t'-t'') \\ &= \frac{2\gamma k_B T e^{-2\frac{k}{\gamma}t}}{\gamma^2}\int_0^t dt' e^{?\frac{k}{\gamma}t'}? \\ &= ?\frac{k_B T e^{-2\frac{k}{\gamma}t}}{k}\left[e^{2\frac{k}{\gamma}t} - \right]? \\ &= ?\frac{k_B T}{k} - \frac{k_B T e^{-2\frac{k}{\gamma}t}}{k} \end{aligned} \tag{29}$$

The third term of the right side in Eq. (27) $\ldots\left\langle \xi_{act}... \right\rangle$ can be solved as follows.

$$\frac{1}{\gamma^2}\int_0^t dt' e^{-\frac{k}{\gamma}(t-t')}\int_0^t dt'' e^{-\frac{k}{\gamma}(t-t'')}\left\langle \xi_{act}(t')\xi_{act}(t'') \right\rangle = \frac{1}{\gamma^2}\int_0^t dt' e^{-\frac{k}{\gamma}(t-t')}\int_0^t dt'' e^{-\frac{k}{\gamma}(t-t'')} C e^{-\left|\frac{t'-t''}{\tau_c}\right|} \tag{30}$$

Here, the time correlation function of the active force $\left\langle \xi_{act}(t')\xi_{act}(t'') \right\rangle = C\mathrm{e}^{-\left|\frac{t'-t''}{\tau_c}\right|}$ is used from Eq. (6). Then, it can be calculated as

$$
\begin{aligned}
&= \frac{C_{\text{외}}}{\gamma^2} e^{-\frac{2k}{\gamma}t} \int_0^t dt' e^{\frac{k}{\gamma}t'} \int_0^t dt'' e^{\frac{k}{\gamma}t''} e^{-\left|\frac{t'-t''}{\tau_c}\right|} \\
&= \frac{C_{\text{외}}}{\gamma^2} e^{-\frac{2k}{\gamma}t} \int_0^t dt' e^{\frac{k}{\gamma}t'} \left[\int_0^{t'} dt'' e^{\frac{k}{\gamma}t''} e^{-\frac{t'-t''}{\tau_c}} + \int_{t'}^t dt'' e^{\frac{k}{\gamma}t''} e^{\frac{t'-t''}{\tau_c}} \right] \\
&= \frac{C_{\text{외}}}{\gamma^2} e^{-\frac{2k}{\gamma}t} \left[\int_0^t dt' e^{\frac{k}{\gamma}t'} \int_0^{t'} dt'' e^{\frac{k}{\gamma}t''} e^{-\frac{t'-t''}{\tau_c}} + \int_0^t dt' e^{\frac{k}{\gamma}t'} \int_{t'}^t dt'' e^{\frac{k}{\gamma}t''} e^{\frac{t'-t''}{\tau_c}} \right].
\end{aligned}
\tag{31}
$$

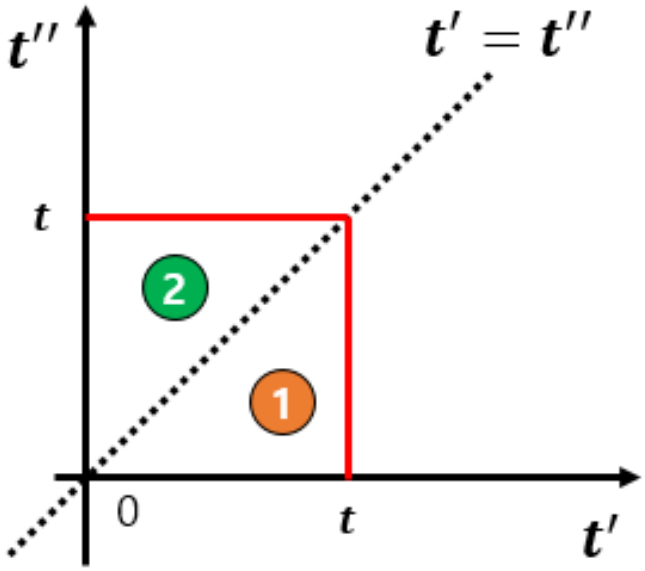

Figure 9: Integral region in Eq. (31)

The integral area of the first term in Eq. (31) represents area 1 in Fig. 9.

$$
\begin{aligned}
Area\,1 &= \int_0^t dt' e^{\left(\frac{k}{\gamma}-\frac{1}{\tau_c}\right)t'} \int_0^{t'} dt'' e^{\left(\frac{k}{\gamma}+\frac{1}{\tau_c}\right)t''} \\
&= \frac{1}{\left(\frac{k}{\gamma}+\frac{1}{\tau_c}\right)} \int_0^t dt' e^{\left(\frac{k}{\gamma}-\frac{1}{\tau_c}\right)t'} \left(e^{\left(\frac{k}{\gamma}+\frac{1}{\tau_c}\right)t'} - \right) \\
&= \frac{1}{\left(\frac{k}{\gamma}+\frac{1}{\tau_c}\right)} \int_0^t dt' \left(e^{\frac{2k}{\gamma}t'} - e^{\left(\frac{k}{\gamma}-\frac{1}{\tau_c}\right)t'} \right) \\
&= \frac{1}{\left(\frac{k}{\gamma}+\frac{1}{\tau_c}\right)} \left[\frac{\gamma}{2k} \left(e^{\frac{2k}{\gamma}t} - 1 \right) - ? \frac{1}{\left(\frac{k}{\gamma}-\frac{1}{\tau_c}\right)} \left(e^{\left(\frac{k}{\gamma}-\frac{1}{\tau_c}\right)t} - \right) \right] \\
&= \frac{\gamma\left(e^{\frac{2k}{\gamma}t} - 1 \right)}{2k\left(\frac{k}{\gamma}+\frac{1}{\tau_c}\right)} - \frac{1}{\left(\frac{k^2}{\gamma^2}-\frac{1}{\tau_c^2}\right)} \left(e^{\left(\frac{k}{\gamma}-\frac{1}{\tau_c}\right)t} - 1 \right) \\
&= \frac{2ke^{\frac{2k}{\gamma}t} - 2ke^{\left(\frac{k}{\gamma}-\frac{1}{\tau_c}\right)t} - ke^{\frac{2k}{\gamma}t} - \frac{\gamma}{\tau_c}e^{\frac{2k}{\gamma}t} + k + \frac{\gamma}{\tau_c}}{2k\left(\frac{k^2}{\gamma^2}-\frac{1}{\tau_c^2}\right)} \\
&= \frac{ke^{\frac{2k}{\gamma}t} - \frac{\gamma}{\tau_c}e^{\frac{2k}{\gamma}t} - k + \frac{\gamma}{\tau_c} - 2ke^{\left(\frac{k}{\gamma}-\frac{1}{\tau_c}\right)t} + 2k}{2k\left(\frac{k^2}{\gamma^2}-\frac{1}{\tau_c^2}\right)} \\
&= \frac{ke^{\frac{2k}{\gamma}t} - \frac{\gamma}{\tau_c}e^{\frac{2k}{\gamma}t} - k + \frac{\gamma}{\tau_c} - 2ke^{\left(\frac{k}{\gamma}-\frac{1}{\tau_c}\right)t} + 2k}{2k\left(\frac{k^2}{\gamma^2}-\frac{1}{\tau_c^2}\right)}
\end{aligned}
\tag{32}
$$

The integral area of the second term in Eq. (31) represents area 2 in Fig. 9.

$$
\begin{aligned}
Area\ 2 &= \int_0^t dt' e^{\left(\frac{k}{\gamma}+\frac{1}{\tau_c}\right)t'} \int_{t'}^t dt'' e^{\left(\frac{k}{\gamma}-\frac{1}{\tau_c}\right)t''} \\
&= \frac{1}{\left(\frac{k}{\gamma}-\frac{1}{\tau_c}\right)} \int_0^t dt' e^{\left(\frac{k}{\gamma}+\frac{1}{\tau_c}\right)t'} \left(e^{\left(\frac{k}{\gamma}-\frac{1}{\tau_c}\right)t} - e^{\left(\frac{k}{\gamma}-\frac{1}{\tau_c}\right)t'} \right) \\
&= \frac{1}{\left(\frac{k}{\gamma}-\frac{1}{\tau_c}\right)} \int_0^t dt' \left(e^{\left(\frac{k}{\gamma}-\frac{1}{\tau_c}\right)t} e^{\left(\frac{k}{\gamma}+\frac{1}{\tau_c}\right)t'} - e^{\frac{2k}{\gamma}t'} \right) \\
&= \frac{1}{\left(\frac{k}{\gamma}-\frac{1}{\tau_c}\right)} \left[e^{\left(\frac{k}{\gamma}-\frac{1}{\tau_c}\right)t} \int_0^t dt' e^{\left(\frac{k}{\gamma}+\frac{1}{\tau_c}\right)t'} - \int_0^t dt' e^{\frac{2k}{\gamma}t'} \right] \\
&= \frac{1}{\left(\frac{k}{\gamma}-\frac{1}{\tau_c}\right)} \left[\frac{e^{\left(\frac{k}{\gamma}-\frac{1}{\tau_c}\right)t}}{\left(\frac{k}{\gamma}+\frac{1}{\tau_c}\right)} \left(e^{\left(\frac{k}{\gamma}+\frac{1}{\tau_c}\right)t} - 1 \right) - \frac{\gamma}{2k} \left(e^{\frac{2k}{\gamma}t} - 1 \right) \right] \\
&= \frac{1}{\left(\frac{k^2}{\gamma^2}-\frac{1}{\tau_c^2}\right)} \left(e^{\frac{2k}{\gamma}t} - e^{\left(\frac{k}{\gamma}-\frac{1}{\tau_c}\right)t} \right) - \frac{\gamma \left(e^{\frac{2k}{\gamma}t} - 1 \right)}{2k \left(\frac{k}{\gamma}-\frac{1}{\tau_c}\right)} \\
&= \frac{2k}{2k\left(\frac{k^2}{\gamma^2}-\frac{1}{\tau_c^2}\right)} \left(e^{\frac{2k}{\gamma}t} - e^{\left(\frac{k}{\gamma}-\frac{1}{\tau_c}\right)t} \right) - \frac{\gamma \left(e^{\frac{2k}{\gamma}t} - 1 \right)\left(\frac{k}{\gamma}+\frac{1}{\tau_c}\right)}{2k\left(\frac{k^2}{\gamma^2}-\frac{1}{\tau_c^2}\right)}
\end{aligned}
\tag{33}
$$

Therefore, the […] in Eq. (24) is the sum of $area\,1$ and $area\,2$ as

$$
\begin{aligned}
area\,1 + area\,2 &= \frac{k e^{\frac{2k}{\gamma}t} - \frac{\gamma}{\tau_c} e^{\frac{2k}{\gamma}t} - k + \frac{\gamma}{\tau_c} - 2k e^{\left(\frac{k}{\gamma}-\frac{1}{\tau_c}\right)t} + 2k}{2k\left(\frac{k^2}{\gamma^2} - \frac{1}{\tau_c^2}\right)} + ? \frac{2k e^{\frac{2k}{\gamma}t} - 2k e^{\left(\frac{k}{\gamma}-\frac{1}{\tau_c}\right)t} - k e^{\frac{2k}{\gamma}t} - \frac{\gamma}{\tau_c} e^{\frac{2k}{\gamma}t} + k + \frac{\gamma}{\tau_c}}{2k\left(\frac{k^2}{\gamma^2} - \frac{1}{\tau_c^2}\right)} \\
&= \frac{k e^{\frac{2k}{\gamma}t} - \frac{\gamma}{\tau_c} e^{\frac{2k}{\gamma}t} - k + \frac{\gamma}{\tau_c} - 2k e^{\left(\frac{k}{\gamma}-\frac{1}{\tau_c}\right)t} + 2k + 2k e^{\frac{2k}{\gamma}t} - 2k e^{\left(\frac{k}{\gamma}-\frac{1}{\tau_c}\right)t} - k e^{\frac{2k}{\gamma}t} - \frac{\gamma}{\tau_c} e^{\frac{2k}{\gamma}t} + k + \frac{\gamma}{\tau_c}}{2k\left(\frac{k^2}{\gamma^2} - \frac{1}{\tau_c^2}\right)} \\
&= \frac{k e^{\frac{2k}{\gamma}t} - \frac{\gamma}{\tau_c} e^{\frac{2k}{\gamma}t} - k + \frac{\gamma}{\tau_c} - 2k e^{\left(\frac{k}{\gamma}-\frac{1}{\tau_c}\right)t} + 2k + 2k e^{\frac{2k}{\gamma}t} - 2k e^{\left(\frac{k}{\gamma}-\frac{1}{\tau_c}\right)t} - k e^{\frac{2k}{\gamma}t} - \frac{\gamma}{\tau_c} e^{\frac{2k}{\gamma}t} + k + \frac{\gamma}{\tau_c}}{2k\left(\frac{k^2}{\gamma^2} - \frac{1}{\tau_c^2}\right)} \\
&= \frac{-4k e^{\left(\frac{k}{\gamma}-\frac{1}{\tau_c}\right)t} + 2k e^{\frac{2k}{\gamma}t} - 2\frac{\gamma}{\tau_c} e^{\frac{2k}{\gamma}t} + 2\frac{\gamma}{\tau_c} + 2k}{2k\left(\frac{k^2}{\gamma^2} - \frac{1}{\tau_c^2}\right)} \\
&= \frac{-2e^{\left(\frac{k}{\gamma}-\frac{1}{\tau_c}\right)t} + e^{\frac{2k}{\gamma}t} - \frac{\gamma}{k\tau_c} e^{\frac{2k}{\gamma}t} + \frac{\gamma}{k\tau_c} + 1}{\left(\frac{k^2}{\gamma^2} - \frac{1}{\tau_c^2}\right)}
\end{aligned}
\tag{34}
$$

Therefore, Eq. (31) is simplified as

$$
\begin{aligned}
&= \frac{C}{\gamma^2} e^{-\frac{2k}{\gamma}t} \left[\frac{-2e^{\left(\frac{k}{\gamma}-\frac{1}{\tau_c}\right)t} + e^{\frac{2k}{\gamma}t} - \frac{\gamma}{k\tau_c} e^{\frac{2k}{\gamma}t} + \frac{\gamma}{k\tau_c} + 1}{\left(\frac{k^2}{\gamma^2} - \frac{1}{\tau_c^2}\right)} \right] \\
&= \frac{C}{\gamma^2} \cdot \frac{-2e^{\left(-\frac{k}{\gamma}-\frac{1}{\tau_c}\right)t} + 1 - \frac{\gamma}{k\tau_c} + \frac{\gamma}{k\tau_c} e^{-\frac{2k}{\gamma}t} + e^{-\frac{2k}{\gamma}t}}{\left(\frac{k^2}{\gamma^2} - \frac{1}{\tau_c^2}\right)} \\
&= \frac{C}{\gamma^2} \tau_c^2 \frac{-2e^{\left(-\frac{k}{\gamma}-\frac{1}{\tau_c}\right)t} + 1 - \frac{\gamma}{k\tau_c} + \frac{\gamma}{k\tau_c} e^{-\frac{2k}{\gamma}t} + e^{-\frac{2k}{\gamma}t}}{\left(\frac{k^2}{\gamma^2}\tau_c^2 - 1\right)}
\end{aligned}
\tag{35}
$$

Here, the intensity of the time-correlation of active force C is $\frac{\gamma^2 D_{act}}{\tau_c}\left(1+\frac{\tau_c}{\tau_k}\right)$.

$$
\begin{aligned}
&= D_{act} t_c \left(1+\frac{\tau_c}{\tau_k}\right) \frac{-2e^{\left(-\frac{k}{\gamma}-\frac{1}{\tau_c}\right)t} + 1 - \frac{\gamma}{k\tau_c} + \frac{\gamma}{k\tau_c} e^{-\frac{2k}{\gamma}t} + e^{-\frac{2k}{\gamma}t}}{\left(\frac{k^2}{\gamma^2}\tau_c^2 - 1\right)} \\
&= D_{act}\left(1+\frac{\tau_c}{\tau_k}\right) \frac{2t_c e^{\left(-\frac{k}{\gamma}-\frac{1}{\tau_c}\right)t} - \tau_c + \frac{\gamma}{k} - \frac{\gamma}{k} e^{-\frac{2k}{\gamma}t} - \tau_c e^{-\frac{2k}{\gamma}t}}{\left(1-\frac{k^2}{\gamma^2}\tau_c^2\right)} \\
&= \frac{D_{act}}{\frac{k}{\gamma}}\left(1+\frac{\tau_c}{\tau_k}\right) \frac{2\frac{k}{\gamma}\tau_c e^{\left(-\frac{k}{\gamma}-\frac{1}{\tau_c}\right)t} - \frac{k}{\gamma}\tau_c + 1 - e^{-\frac{2k}{\gamma}t} - \frac{k}{\gamma}\tau_c e^{-\frac{2k}{\gamma}t}}{\left(1-\frac{k^2}{\gamma^2}\tau_c^2\right)} \\
&= \frac{D_{act}}{\frac{k}{\gamma}}\left(1+\frac{\tau_c}{\tau_k}\right) \frac{1 - e^{-\frac{2k}{\gamma}t} - \frac{k}{\gamma}\tau_c\left(1 + e^{-\frac{2k}{\gamma}t} - 2e^{\left(-\frac{k}{\gamma}-\frac{1}{\tau_c}\right)t}\right)}{\left(1-\frac{k^2}{\gamma^2}\tau_c^2\right)}
\end{aligned}
\tag{36}
$$

Here, $D_{act} \equiv k_B T_{act}/\gamma$ is the active diffusion coefficient whose physical meaning will be explained in Section 4.1. Therefore, the dispersion of the particle position is

$$
\begin{aligned}
\left\langle x(t)^2 \right\rangle &= \left\langle x_0^2 \right\rangle e^{-\frac{2k}{\gamma}t} + \frac{k_B T}{k} - \frac{k_B T e^{-2\frac{k}{\gamma}t}}{k} \\
&+ \frac{k_B T_{act}}{k}\left(1+\frac{\tau_c}{\tau_k}\right) \frac{1 - e^{-\frac{2k}{\gamma}t} - \frac{k}{\gamma}\tau_c\left(1 + e^{-\frac{2k}{\gamma}t} - 2e^{\left(-\frac{k}{\gamma}-\frac{1}{\tau_c}\right)t}\right)}{\left(1-\frac{k^2}{\gamma^2}\tau_c^2\right)}.
\end{aligned}
\tag{37}
$$

Here, T_{act} is $D_{act}\gamma/k_B$ and the dispersion of position at the initial time $\left\langle x_0^2 \right\rangle$ can't use the equipartition theorem any more. Because the system with active force is not satisfied as thermal equilibrium state

$$\left\langle x_0^2 \right\rangle \neq \frac{k_B T}{k} \tag{38}$$

In a steady-state condition, the dispersion of particle position $\left\langle x(t)^2 \right\rangle$ is constant.

$$\begin{aligned} \therefore lim_{t\to\infty}\left\langle x(t)^2 \right\rangle = lim_{t\to\infty}\Bigg[& \left\langle x_0^2 \right\rangle e^{-\frac{2k}{\gamma}t} + \frac{k_B T}{k} - \frac{k_B T e^{-2\frac{k}{\gamma}t}}{k} \\ & + \frac{k_B T_{act}}{k}\left(1+\frac{\tau_c}{\tau_k}\right)\frac{1-e^{-\frac{2k}{\gamma}t} - \frac{k}{\gamma}\tau_c\left(1+e^{-\frac{2k}{\gamma}t} - 2e^{\left(-\frac{k}{\gamma}-\frac{1}{\tau_c}\right)t}\right)}{\left(1-\frac{k^2}{\gamma^2}\tau_c^2\right)}\Bigg] \\ = & \frac{k_B T}{k} + \frac{k_B T_{act}}{k}\left(1+\frac{\tau_c}{\tau_k}\right)\frac{1-\frac{k}{\gamma}\tau_c}{\left(1-\frac{k^2}{\gamma^2}\tau_c^2\right)} \\ = & \frac{k_B T}{k} + \frac{k_B T_{act}}{k}\left(1+\frac{\tau_c}{\tau_k}\right)\frac{1}{\left(1+\frac{k}{\gamma}\tau_c\right)} \end{aligned} \tag{39}$$

.

Therefore, the dispersion of the particle position in the steady condition is

$$\therefore \left\langle x_{s.s.}^2(t) \right\rangle = \frac{k_B T}{k} + \frac{k_B T_{act}}{k}\left(1+\frac{\tau_c}{\tau_k}\right)\frac{1}{\left(1+\frac{k}{\gamma}\tau_c\right)}. \tag{40}$$

Therefore, the mean square displacement in the steady-state is expressed as

$$\left\langle \left[x(t)-x(0)\right]^2 \right\rangle = 2\left\langle x^2(t) \right\rangle - 2\left\langle x(t)x(0) \right\rangle. \tag{41}$$

Here, the dispersion $\left\langle x^2(t) \right\rangle$ and $\left\langle x^2(0) \right\rangle$ are the same in the steady-state. Using Eq. (24) and Eq. (40),

$$\left\langle \left[x(t)-x(0) \right]^2 \right\rangle = 2\left[\frac{k_B T}{k} + \frac{k_B T_{act}}{k}\left(1+\frac{\tau_c}{\tau_k}\right)\frac{1}{\left(1+\frac{k}{\gamma}\tau_c\right)} \right]$$

$$- 2\left[\frac{k_B T}{k} e^{-\frac{t}{\tau_k}} + \frac{k_B T_{act}}{k}\cdot\left(1+\frac{\tau_c}{\tau_k}\right)\frac{e^{-\frac{t}{\tau_k}} - \frac{\tau_c}{\tau_k} e^{-\frac{t}{\tau_c}}}{1-\frac{\tau_c^2}{\tau_k^2}} \right] \qquad (42)$$

$$= 2\left(\frac{k_B T}{k}\right)\left(1-e^{-t/\tau_k}\right) + 2\left(\frac{k_B T_{act}}{k}\right)\frac{\left[1-e^{-t/\tau_k} - \left(\frac{\tau_c}{\tau_k}\right)\left(1-e^{-t/\tau_c}\right)\right]}{\left(1-\frac{\tau_c}{\tau_k}\right)}.$$

IV Experiment result

4.1 Enhanced mobility with the active force.

The mean square displacement (MSD) of the particle position during the elapsed time t can be found as

$$<\Delta x^2(t)> = 2\left(\frac{k_B T}{k}\right)\left(1-e^{-t/\tau_k}\right) + 2\left(\frac{k_B T_{act}}{k}\right)\frac{\left[1-e^{-t/\tau_k}-\left(\frac{\tau_c}{\tau_k}\right)\left(1-e^{-t/\tau_c}\right)\right]}{\left(1-\frac{\tau_c}{\tau_k}\right)}. \quad (43)$$

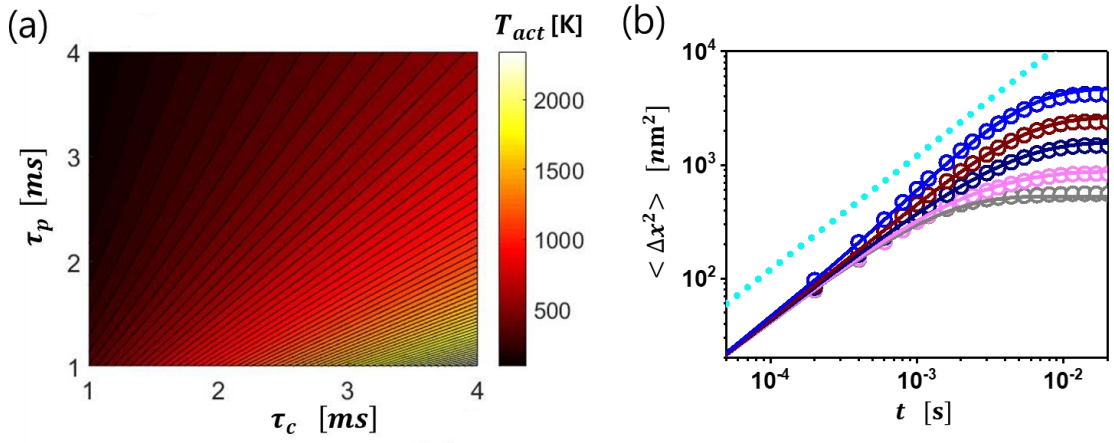

Figure 10: Active temperature T_{act} and Mean square displacement (MSD) of a tracer particle in an active bath. (a) Phase map of active temperature (simulation) for various τ_c and τ_c with fixed $X = 37m$m . (b) Mean square displacement (MSD) of tracer particle with the active force. Double logarithmic schematic representation of a tracer particle MSDs, for various conditions τ_p : $1ms$ (blue), $2ms$ (brown), $4ms$ (navy), and $12ms$ (pink). The gray hollow circle represents the MSD without the active noise. Here, $X = 37$ nm, $\tau_c = 4$ ms, and $\tau_k = 1.1$ ms. The hollow circles represent experimental results and the splines are predictions using Eq. (43). The cyan dotted line represents the slope of unity corresponding to the free diffusion.

with active force in a thermal bath in steady-state. The derivation is given in Section 3.4. Here, $T_{act} = kX^2\tau_c^2\left(1+\tau_c/\tau_k\right)^{-1}/2k_B\tau_p\tau_k$ is "active temperature" which quantifies how the active noise boosts the mobility of the tracer.[31] Figure 10 (a) shows the active temperature for various τ_c and τ_p with fixed random kick amplitude X . When the elapsed time t is much less than τ_c and τ_k, MSD is proportional to time t given as $2D_{th}t$, because only thermal noise is dominant in this

regime. In the long time regime ($t >> \tau_k$ and τ_c), the mean square displacement is saturated at $\left\langle \Delta x^2(t) \right\rangle = 2\left(k_B/k\right)\cdot(T+T_{act})$. Since $T_{act} = \gamma D_{act}/k_B$, the higher active temperature means the larger active diffusion coefficient that represents the degree of movement only by the active force. Since the active force is uncorrelated to the thermal noise,[32] the diffusion of the particle due to the active force is independent of that due to the thermal noise.[31]

Fig. 10 (b) shows the mean square displacement data at various active force conditions. The MSD data represented as gray hollow circles is for the thermal equilibrium condition without active forces. All colored hollow circles correspond to the experimental MSD data with fixed parameter values $\left(\tau_c, X^2\right)$, but different average kick interval time τ_p in non-equilibrium steady-state. The experimental MSD data is well-agreed with the theoretical predictions in Eq. (43) as a function of τ_p. When the average kick interval time τ_p is decreased while the kick duration time τ_c is fixed, the number of kicks per unit time increases, so the active temperature T_{act} increases. Also, as shown in Fig. 10 (b), the MSD value is saturated $2\left\langle x^2(t)\right\rangle$ at the long time limit. From this value, we can easily measure the active temperature T_{act}.[33] The cyan dotted line represents the MSD slope when the particles diffuse freely.

To understand the time-dependent properties of MSD in the presence of active force, we can simplify Eq. (43),

$$< \Delta x^2(t) > = A\left(1-\mathrm{e}^{-t/\tau_k}\right) - B\left(1-\mathrm{e}^{-t/\tau_c}\right). \tag{44}$$

Here, $A \equiv \left(2\frac{k_B T}{k} + 2\frac{k_B T_{act}}{k\left(1-\tau_c/\tau_k\right)} \right)$, $B \equiv \frac{2k_B T_{act}}{k\left(1-\tau_c/\tau_k\right)}\frac{\tau_c}{\tau_k}$, and $A > B$ always. From Eq. (44), the MSD shows interesting results depending on the ratio of τ_c and τ_k. Fig. 11 (a) shows the MSD for the case of $\tau_c << \tau_k$. In the limit of $t \geq \tau_k$, MSD becomes a single exponentially increasing function of $< \Delta x^2(t) > = A - B - A\mathrm{e}^{-t/\tau_k}$. In this case, the motion of tracer particle in the short time ($t \approx \tau_c$) is determined by thermal noise and active noise, but in the long time ($t \geq \tau_k$) the motion is is determined by optical trapping time τ_k. Fig. 11 (b) shows the MSD for the case of $\tau_k << \tau_c$. In the limit of $t \geq \tau_c$, MSD becomes $< \Delta x^2(t) > = A - B + B\mathrm{e}^{-t/\tau_c}$. In the short time ($t \approx \tau_k$), the tracer particle is only affected by thermal noise and harmonic potential such as without an active noise environment. In the long time $t \geq \tau_c$ regime, the tracer is primarily affected by the active force and thermal force. Therefore, the MSD is exponentially saturated near $t \sim \tau_c$.

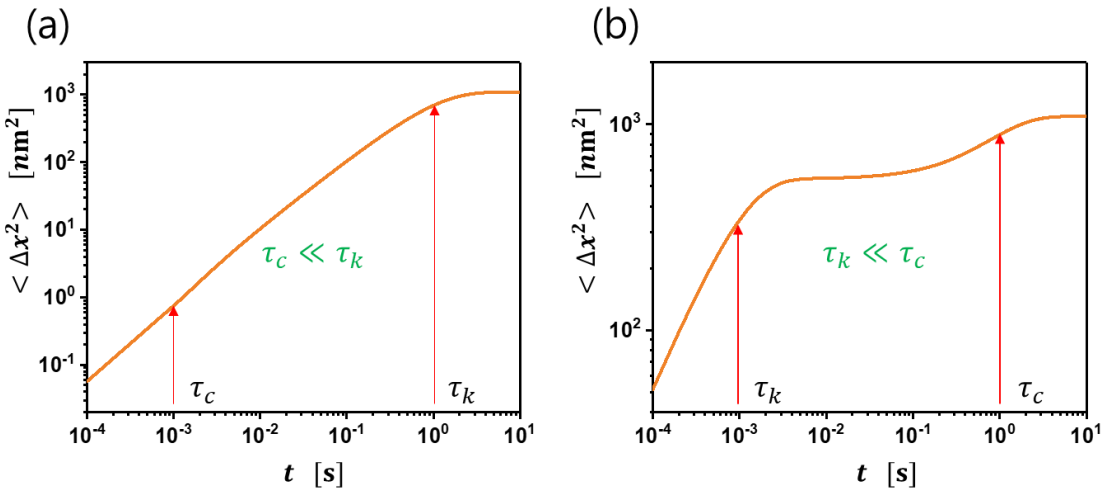

Figure 11: Mean square displacement for two extreme ratio of τ_c and τ_k from Eq. (44). (a) In the case of $\tau_c \ll \tau_k$, the MSD shows an exponentially saturating form. Here, the conditions are $T = 300K$, $T_{act} = 300K$, $\tau_c = 1ms$, and $\tau_k = 1s$. (b) In the case of $\tau_c \gg \tau_k$, the MSD shows a double exponential form. Here, conditions are $T = 300K$, $T_{act} = 300K$, $\tau_c = 1s$, and $\tau_k = 1ms$.

4.2 (Non-) Gaussian diffusion with the active force.

Figure 12 shows the probability density functions $P(x)$ of the tracer particle position in steady-state for various τ_p with fixed τ_c and X. As we mentioned in Chapter I, In case of $\tau_c/\tau_p \gtrsim 1$, $P(x)$ shows a Gaussian distribution. However, $P(x)$ shows a non-Gaussian for $\tau_c/\tau_p < 1$. In the latter case, $P(x)$ has an exponential behaviour at tails but a Gaussian behaviour near the center. In order to quantify the degree of non-Gaussianity[34], we measure the non-Gaussian parameter $\alpha_2 \equiv [< x^4 > / 5 < x^2 >^2] - 3/5$ which is related to kurtosis. The closer the non-Gaussian parameter to 0, the closer the $P(x)$ to the Gaussian distribution. In case of $\tau_c/\tau_p \gtrsim 1$, $P(x)$ follows always Gaussian behavior ($\alpha_2 \approx 0$) as shown in the inset of Fig. 12 (b). And, for $0 < \tau_c/\tau_p < 1$, $P(x)$ shows non-Gaussian behavior ($\alpha_2 > 0$). But, in the limit $\tau_c/\tau_p \approx 0$, $P(x)$ becomes Gaussian ($\alpha_2 \approx 0$) again, because the number of active force events at a given time is remarkably small. This result agrees with real bio-active experiments in which the PDF shows non-Gaussian distribution when the concentration of active particles in the surrounding medium is low, corresponding to $\tau_c/\tau_p < 1$.[7] Detailed comparison is in Section 4.3.

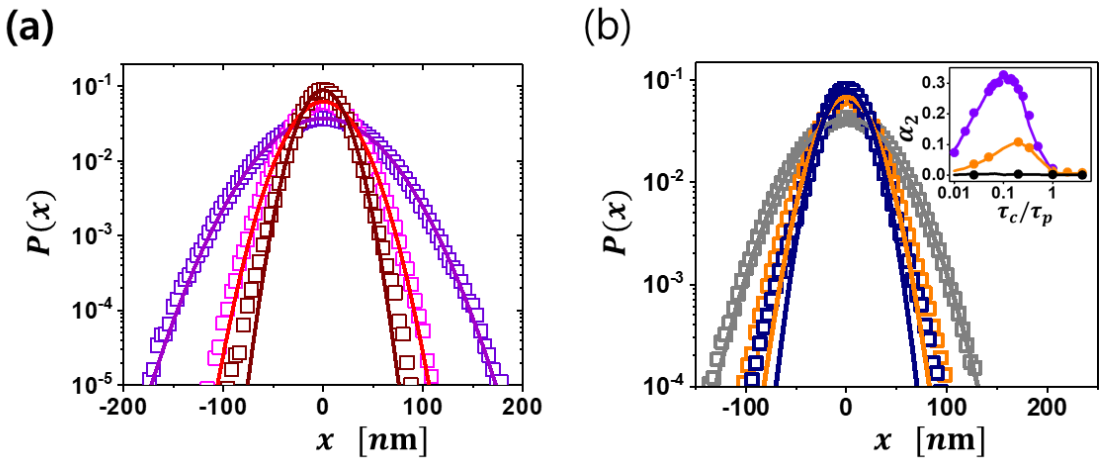

Figure 12: Probability distribution function (PDF) of tracer under active force. (a) PDFs are plotted for τ_p: 1*m*s (Purple), 4 *m*s (pink), and 20 *m*s (brown) for $X = 37\,nm$ and $\tau_c = 4\,ms$. (b) PDFs are plotted for τ_p: 2*m*s (gray), 6*m*s (orange), and 10*m*s (navy) for $X = 70\,nm$ and $\tau_c = 2\,ms$. The solid splines are Gaussian fits. The inset plots the non-Gaussian parameter α_2 against τ_c/τ_p. The hollow circles are from experiments and the splines are simulation data. Here, $X = 70\,nm$ (violet), $37\,nm$ (orange), $20\,nm$ (black) and $\tau_c = 2\,ms$ (violet, black), $4\,ms$ (orange).

To explain these observations, we analyze the motion of the particle by separating them into two independent parts. One is the motion $x_{th} \equiv x - x_{act}$ caused by the thermal noise and the other is the motion x_{act} caused by the active force. Therefore, $P(x)$ can be shown as the convolution of $P(x_{th})$ and $P(x_{act})$ as $P(x) = \int P(x_{th})P(x_{act})dx_{act}$.[35] Here, the $P(x_{th})$ by thermal noise in the harmonic potential is as follows: $P(x_{th}) = \sqrt{k/2\pi k_B T}\ \mathrm{e}^{-kx_{th}^2/2k_B T}$. In order for $P(x)$ to show a non-Gaussian property, $P(x_{act})$ must have a non-Gaussian distribution ($\tau_c/\tau_p < 1$). However, if the tails of $P(x_{act})$ do not surpass roughly 4σ (4 standard deviations) of $P(x_{th})$, $P(x)$ at a glance it still looks like having a Gaussian distribution as shown in Fig.14 (b). It is caused by the equilibration process of the particle position, located inside the harmonic potential that wipes out the non-Gaussian effect of the active noise. Interestingly, under this conditions, even though $P(x)$ shows a Gaussian distribution, the van Hove self-correlation function $G_s(\Delta x, \Delta t)$, which is the PDF of the particle displacement Δx during Δt, shows a non-Gaussian distribution at a shorter time regime in Fig.13. In this figure, for small Δt, $\alpha_2 \approx 0$. This is due to the free diffusion as shown in Fig. 10 (b). For large Δt, $\alpha_2 \approx 0$. This is result of the central limit theorem. Currently, the non-Gaussian tail is explained by theory considering the hydrodynamic interactions between the tracer particle and the active particles. Additionally, the active

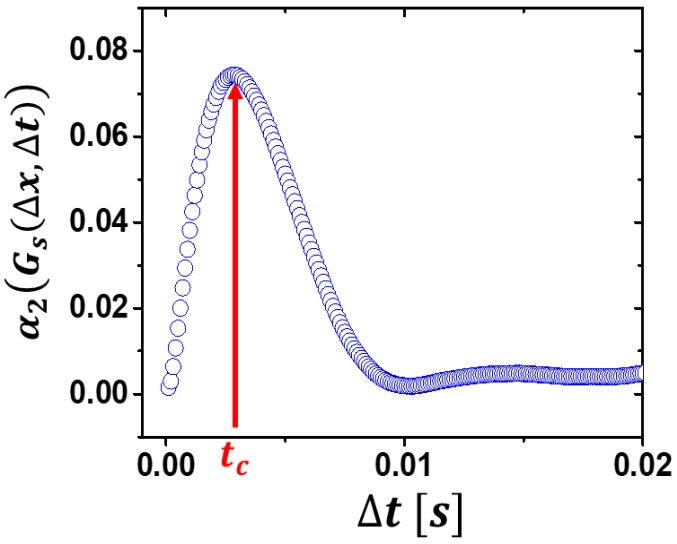

Figure 13: The non-Gaussian parameter value of van Hove self-correlation function $G_s(\Delta x, \Delta t)$ vs. Δt. α_2 is obtained by computer simulation for $X = 70nm$, $\tau_c = 0.3ms$, and $\tau_k = 0.8ms$. In the same condition, the non-Gaussian parameter value of $P(x)$ is 0.

force is arriving at random intervals, determined by Poisson distribution.[36] The approach taken here complements that rigorous but complex analysis.

Since the system is in thermal equilibrium always, the PDF of x_{th} remains Boltzmann every time, and hence that of $x - x_{act}(t)$ for a given $x_{act}(t)$ such that

$$P(x,t \mid x_{act}) = \sqrt{\frac{k}{2\pi k_B T}}\, \mathrm{e}^{-k\left(x - x_{act}(t)\right)^2 / 2k_B T}. \tag{45}$$

This conditional PDF of x for $x_{act}(t)$ is Gaussian, while the PDF averaged over $x_{act}(t)$ becomes non-Gaussian in general. From Eq. (5), we have

$$x_{th}(t) = \frac{1}{\gamma}\int_0^t ds \mathrm{e}^{-(t-s)/\tau_k}\xi_{th}(s), \quad x_{act}(t) = \frac{1}{\gamma}\int_0^t ds \mathrm{e}^{-(t-s)/\tau_k}\xi_{act}(s). \tag{46}$$

The variance of each position is calculated from Eqs. (8) and (46) in the long-time limit $t \gg \tau_c$, given as

$$\left\langle x_{th}^2 \right\rangle = \frac{k_B T}{k}, \quad \left\langle x_{act}^2 \right\rangle = \frac{X^2}{2}\frac{\tau_c}{\tau_p}\left(1 + \frac{\tau_k}{\tau_c}\right)^{-1} = \frac{k_B T_{act}}{k}, \tag{47}$$

where T_{act} is the active temperature which quantifies the tracer activity owing to the presence of the active force. Then, we find the variance of $x = x_{th} + x_{act}$ as

$$\left\langle x^2 \right\rangle = \left\langle x_{th}^2 \right\rangle + \left\langle x_{act}^2 \right\rangle = \frac{k_B\left(T + T_{act}\right)}{k}. \tag{48}$$

The full statistics requires the information of all the moments of higher orders due to a non-Gaussian property of x_{act}, which is practically impossible. Fig. 14 shows the PDFs of x, x_{act}, and x_{th}. For large τ_c/τ_p, $P(x_{act})$ and $P(x)$ are close to Gaussian distributions because a large number of kicks during the correlation time τ_c causes Gaussian due to the central limit theorem. This was discussed analytically in Section 3.1. When $\tau_c/\tau_p \ll 1$, $P(x)$ shows non-Gaussian with large side-tails. But according to the inset of Fig. 12.2 (b), the non-Gaussian parameter $\alpha_2 \approx 0$ in this regime. This is due to the very small values of $P(x)$ (order of $10^{-3} \sim 10^{-5}$) at the side-tails whose contribution to α_2 is negligibly small.

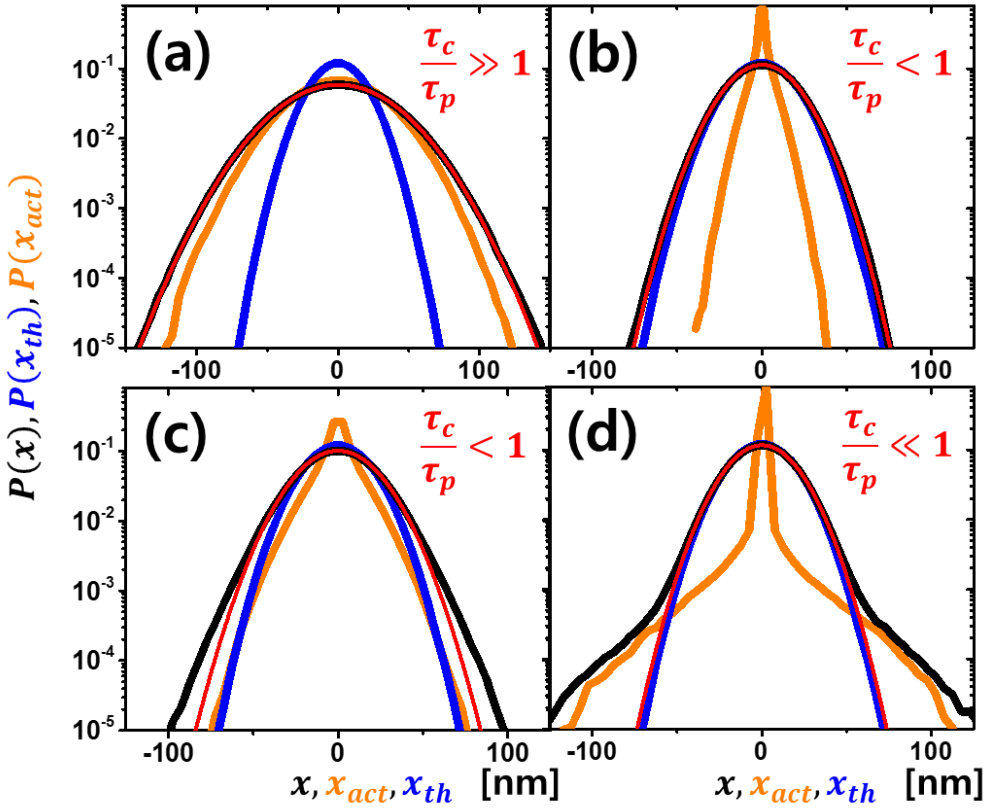

Figure 14: PDFs of particle position. PDFs of x (black), x_{act} (orange), and x_{th} (blue) from Eq. (1) and Eq. (S2) by using computer simulation. The red solid curves are Gaussian fittings to $P(x)$. (a) and (b) show the PDFs when $P(x)$ is Gaussian-like. (c) and (d) show the PDFs when $P(x)$ is non-Gaussian. The conditions are (a) $X = 20\,nm$, $\tau_c = 10\,ms$ and $\tau_p = 2\,ms$, (b) $X = 20\,nm$, $\tau_c = 2\,ms$ and $\tau_p = 10\,ms$, (c) $X = 40\,nm$, $\tau_c = 2\,ms$ and $\tau_p = 8\,ms$, and (d) $X = 70\,nm$, $\tau_c = 4\,ms$ and $\tau_p = 200\,ms$. $\tau_c = 4\,ms$ and $\tau_p = 200\,ms$.

We mentioned $P(x)$ is always Gaussian-like near the center position where $|x| < k_B T / k$ even under high active temperature. This property can be explained from Eq. (45) as

$$P(x) = \sqrt{\frac{k}{2\pi k_B T}} e^{-\frac{kx^2}{2k_B T}} \int \left(e^{\frac{kxx_{act}}{k_B T} - \frac{kx_{act}^2}{2k_B T}} \right) P(x_{act})\, dx_{act} \tag{49}$$

After using the Taylor expansion inside the integration term,

$$
\begin{aligned}
P(x) &= \sqrt{\frac{k}{2\pi k_B T}} e^{\frac{-kx^2}{2k_B T}} \int \left[1 + \frac{kx}{k_B T} x_{act} + \frac{1}{2!}\left(\frac{kx}{k_B T}\right)^2 x_{act}^2 + \right. \\
&\qquad \left. \cdots + \frac{1}{n!}\left(\frac{kx}{k_B T}\right)^n x_{act}^n \right] e^{-\frac{kx_{act}^2}{2k_B T}} P\left(x_{act}\right) dx_{act} \\
&= \sqrt{\frac{k}{2\pi k_B T}} e^{\frac{-kx^2}{2k_B T}} \left[\int_{-\infty}^{\infty} e^{-\frac{kx_{act}^2}{2k_B T}} P\left(x_{act}\right) dx_{act} + \frac{1}{2!}\left(\frac{kx}{k_B T}\right)^2 \int_{-\infty}^{\infty} x_{act}^2 e^{-\frac{kx_{act}^2}{2k_B T}} P\left(x_{act}\right) dx_{act} + \right. \\
&\qquad \left. \cdots + \frac{1}{n!}\left(\frac{kx}{k_B T}\right)^n \int_{-\infty}^{\infty} e^{-\frac{kx_{act}^2}{2k_B T}} P\left(x_{act}\right) dx_{act} \right]
\end{aligned}
\tag{50}
$$

If we see the position near the center, which satisfies the condition $kx < k_B T$, we can ignore the high order $\left(kx/k_B T\right)$ terms. Therefore, Eq. (50) becomes

$$
\begin{aligned}
P\left(x\right) &\approx \sqrt{\frac{k}{2\pi k_B T}} e^{\frac{-kx^2}{2k_B T}} \int_{-\infty}^{\infty} \mathrm{e}^{-\frac{kx_{act}^2}{2k_B T}} P\left(x_{act}\right) dx_{act} \\
&= A e^{\frac{-kx^2}{2k_B T}}
\end{aligned}
\tag{51}
$$

Therefore, the central part of the PDF always shows a Gaussian distribution.

4.3 Real bio-active vs. active force model

There are many studies related to the dynamic of real experimental bio-active matter or environment.[37-41] In order to test our model with the real experimental bio-active matter, we chose the experimental work by J. Gollub et. al. They studied the enhanced diffusion of tracer particles in a quasi-two-dimensional bath of swimming Chlamydomonas (algal cell) using the video-imaging analysis. They measured the mean square displacement and van Hove self-correlation function of tracer particles as function of volume fraction of cell Φ.[3] The cell concentration was controlled by 3D volume fraction Φ from the low concentration of $\Phi = 0.3\%$ to the high concentration of 7%. Figure 18 (a) shows that the van Hove self-correlation function $G_s(\Delta x, \Delta t)$ switches from non-Gaussian to Gaussian distribution depending on the volume fraction.

Since there is no harmonic potential in this experiment ($k = 0$), to apply our model to this experiment, Eq. (1) needs to be modified as $\gamma \dot{x} = \xi_{th}(t) + \xi_{act}(t)$. The position of the tracer particle is simply expressed as

$$\Delta x(t) = \frac{1}{\gamma}\int_0^t dt' \left[\xi_{th}(t') + \xi_{act}(t')\right], \tag{52}$$

and the MSD of the tracer particles $\left\langle \Delta x^2(t) \right\rangle$ is

$$\left\langle \Delta x^2(t) \right\rangle = \frac{1}{\gamma^2}\int_0^t dt' \int_0^t dt'' \left\langle \xi_{th}(t')\xi_{th}(t'') \right\rangle + \frac{1}{\gamma^2}\int_0^t dt' \int_0^t dt'' \left\langle \xi_{act}(t')\xi_{act}(t'') \right\rangle. \tag{53}$$

Using $\left\langle \xi_{th}(t')\xi_{th}(t'') \right\rangle = 2\gamma k_B T \delta(t'-t'')$, $\left\langle \xi_{act}(t')\xi_{act}(t'') \right\rangle \equiv C\mathrm{e}^{-\left|\frac{t'-t''}{\tau_c}\right|}$, and $C = \gamma^2 \frac{D_{act}}{\tau_c} = \frac{f_{RMS}^2 \tau_c}{2\tau_p}$, Here, the f_{RMS} is defined as root-mean-square (RMS) random active kick force. (In harmonic potential, the active force satisfies this relationship by putting $f_{RMS} = kX$) Then, we can simplify Eq. (53) as

$$\left\langle \Delta x^2(t) \right\rangle = 2\frac{k_B T}{\gamma} t + \frac{2C\tau_c}{\gamma^2}\int_0^t dt' \mathrm{e}^{-t'/\tau_c}\left(\mathrm{e}^{t'/\tau_c} - 1\right). \tag{54}$$

Finally, the MSD of the tracer particles in an active bath is expressed as

$$\left\langle \Delta x^2(t) \right\rangle = 2D_{th}t + 2D_{act}\left[t - \tau_c\left(1 - e^{-t/\tau_c}\right)\right], \tag{55}$$

Here $D_{th} = k_B T/\gamma$ is the thermal diffusion coefficient and $D_{act} = f_{RMS}^2 \tau_c^2 / \left(2\gamma^2 \tau_p\right)$ is the active diffusion coefficient. Figure 15 shows the MSD function by using Eq. (20). In two extreme time scales, a short time $t \ll \tau_c$ and long time regime $t \gg \tau_c$, the tracer particle behavior shows the free Brownian

motion, because of $\langle \Delta x^2(t) \rangle \propto t$. In a short time case, there is not enough time for the tracer particle to feel the active force. According to the central limit theorem, the tracer behavior shows Brownian motion in a long time regime. However, when the time scale is near the kick duration time $t \approx \tau_c$, the MSD shows superdiffusion as $\langle \Delta x^2(t) \rangle \propto t^\alpha$ with $\alpha > 1$, because the active force boosts the mobility of the tracer in this time scale. The violet dotted line represents free diffusion, showing the unity slope.

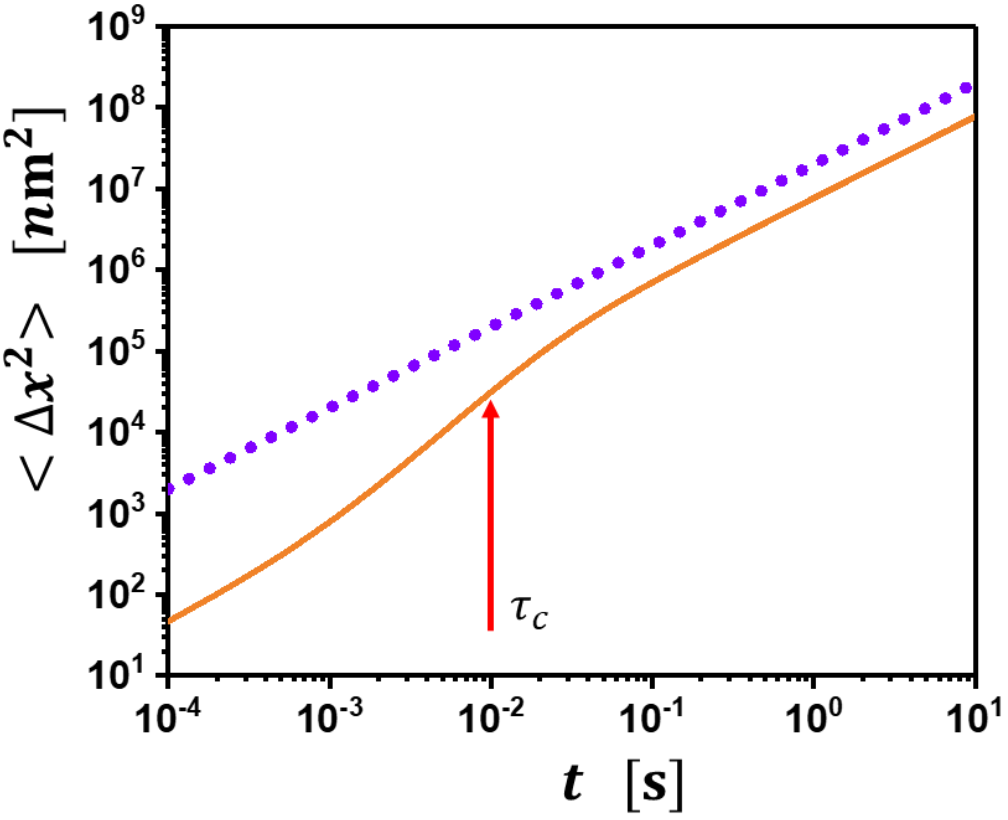

Figure 15: The MSD drawn by using Eq. (55). Here, the condition used is $T = 300K$, $T_{act} = 3000K$, and $\tau_c = 10ms$. It shows superdiffusion motion only near $t \approx \tau_c$. The violet dotted line represents free diffusion, showing the unity slope.

By fitting Eq. (55) to the experimental MSD data obtained by J. Gollub as shown in Fig. 16, we estimated the kick duration $\tau_c = 0.3$s and D_{act} for different cell volume fraction Φ . We conduct a computer simulation based on our model with the fitted parameters of $\tau_c = 300ms$ and D_{act} as shown in Fig. 16. We find that the $G_s(\Delta x, \Delta t)$ (splines) from the simulation is well-agreed with the data

measured by J. Gollub (colored hollow circles) when the random kicking force $f_{RMS} = 0.4$ pN and the average kick interval time satisfies the relation $\tau_p \sim \Phi^{-3/2}$.

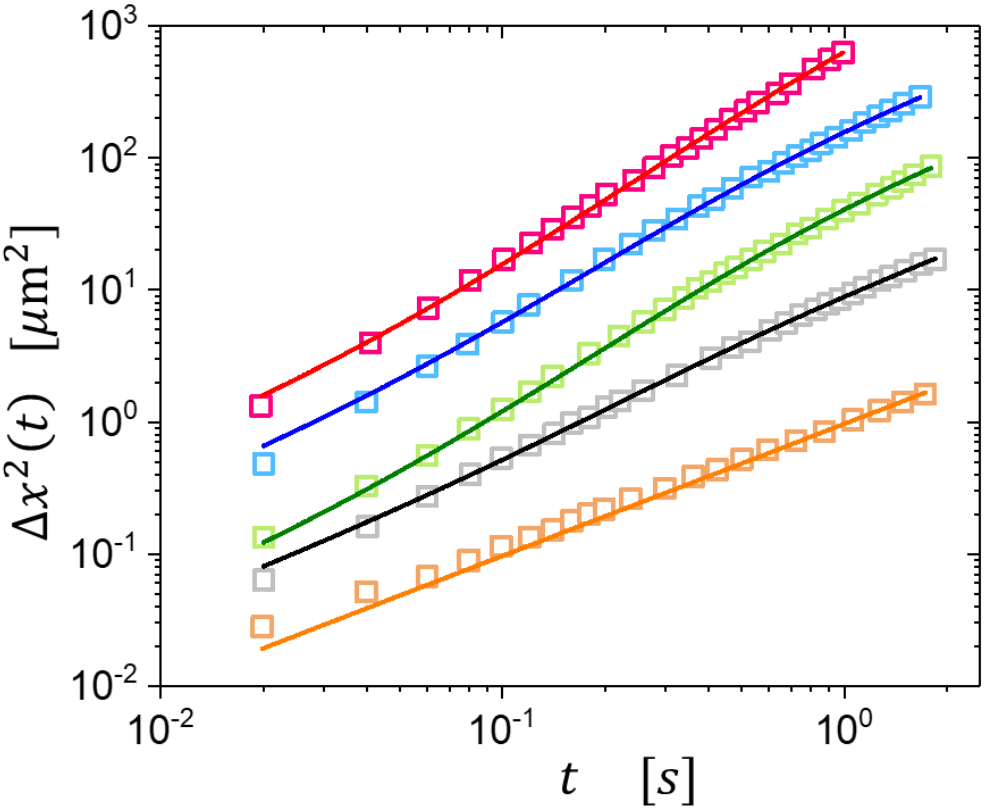

Figure 16: Mean square displacement (MSD) of 1μm polystyrene beads in an active bath and fitting curves. All colored hollow squares represent the experimental work by J. Gollub et. al. Here, the cell volume fraction $\Phi = 0\%$ (orange), 0.3% (gray), 0.7% (green), 2.7% (blue) and $\Phi = 7.0\%$ (red).

To understand this relation $\tau_p \sim \Phi^{-3/2}$, we assume a situation where the cells are swimming in a cube of length L. In this case, the definition of volume fraction of cells Φ is expressed as

$$\Phi = \frac{NV_c}{V} = \frac{N}{L^3}\frac{4}{3}\pi r_c^3 \tag{56}$$

in Fig. 17. Here, the N is the number of active cells, V_c is the average volume of the cell, and r_c is the average radius of the cell. In the experiment, all the cells are sedimented at the bottom. Therefore, the experiment was done in 2D geometry. According to our model, we assume that the concentration of active particles is inversely proportional to the average kick interval time τ_p. Since the total number of

the cells is a fixed value N, the 2D concentration ρ has a relation with the 3D volume fraction Φ. The area fraction in 2D geometry is the 2D concentration.

$$\rho = \frac{NV_c}{A} = \frac{N}{L^2}\pi r_c^2. \tag{57}$$

From Eq. (56) and Eq. (57), $\rho \propto \Phi^{3/2}$. Since the average time interval between kicks τ_p is related with the concentration of the cell, the τ_p is expressed as $\tau_p \sim \rho^{-1} \sim \Phi^{-3/2}$.

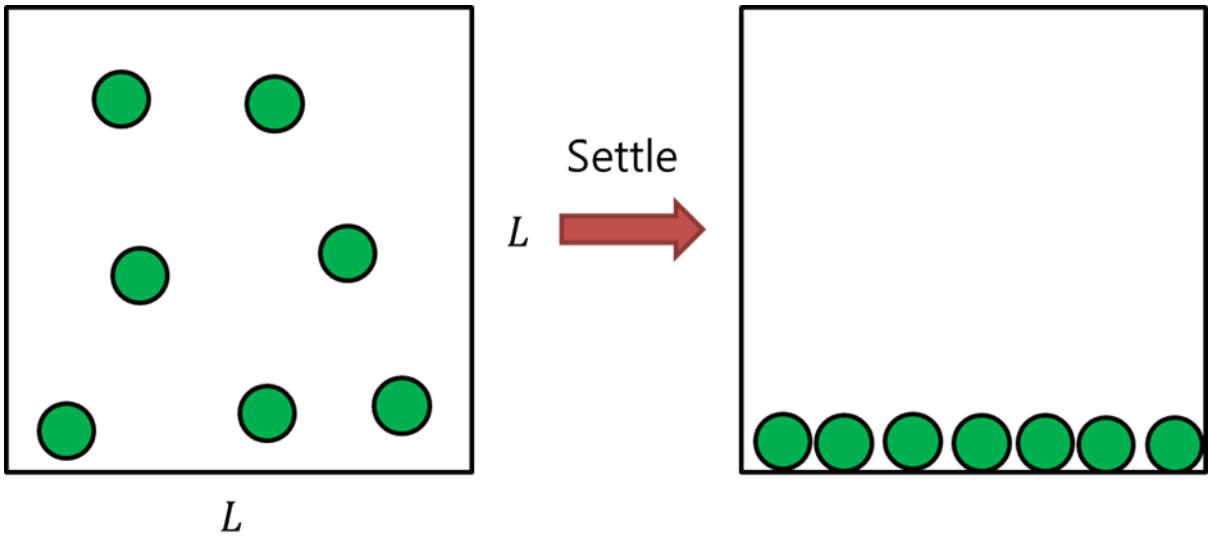

Figure 17: N number of swimming active cells in the 3D box of length L. Here, the green circles represent each cell.

In the experiment, the van Hove self-correlation function $G_s(\Delta x, \Delta t)$ shows Gaussian-like for high cell concentration and non-Gaussian for low cell concentration. We find that when there are many collision events between the active cells and the tracer particles due to the high cell concentration, $G_s(\Delta x, \Delta t)$ becomes Gaussian distribution, corresponding to $\tau_c/\tau_p \gtrsim 1$. On the other hand, when the collisions are rare, $\tau_c/\tau_p < 1$, $G_s(\Delta x, \Delta t)$ becomes non-Gaussian behavior. In the experiment, $D_{eff} \propto \Phi^{3/2}$. If we assume that the diffusion is dominated by the active particle, $D_{eff} = D_{th} + D_{act} \approx D_{act}$. According to our model $D_{act} \sim \tau_p^{-1}$. Therefore, $D_{eff} \approx D_{act} \sim \tau_p^{-1}$. This explains the simulation using our model agrees well with the experimental data as shown in Fig.18 (a). Figure 18 (b) shows that the effective diffusion coefficient $D_{eff} \sim \Phi^{3/2}$ in the experiment and $D_{act} \sim \tau_p^{-1} \sim \Phi^{3/2}$.

In the experiment the average speed of the cell movement is $v_0 \approx 100\,\mu\mathrm{m/s}$. In order to understand that the random kicking force $f_{RMS} = 400\ n\mathrm{N}$, we assumed that the instantaneous speed of the tracer particle is the average speed of the cell when the cell is interacting with the tracer particle. In this case, the average drag force which the tracer particle feels is the Stokes force satisfying $\gamma v_0 = 6\pi a \eta v_0 \approx 0.4\,p\mathrm{N}$. Here, a is the diameter of tracer ($1\mu\mathrm{m}$) and η is the viscosity of the surrounding medium. This average drag force is the same as the fitted $f_{RMS} = 400\ n\mathrm{N}$.

The above comparison between the real bio-active matter system and the active force model suggests that although our active force model does not include mechanics of the active bath in details. These mechanics include hydrodynamics – e.g. interactions between the tracer and active particles[36] and among the active particles, it can explain very well the enhanced diffusion and (non-) Gaussian statistics in the real bio-active bath.

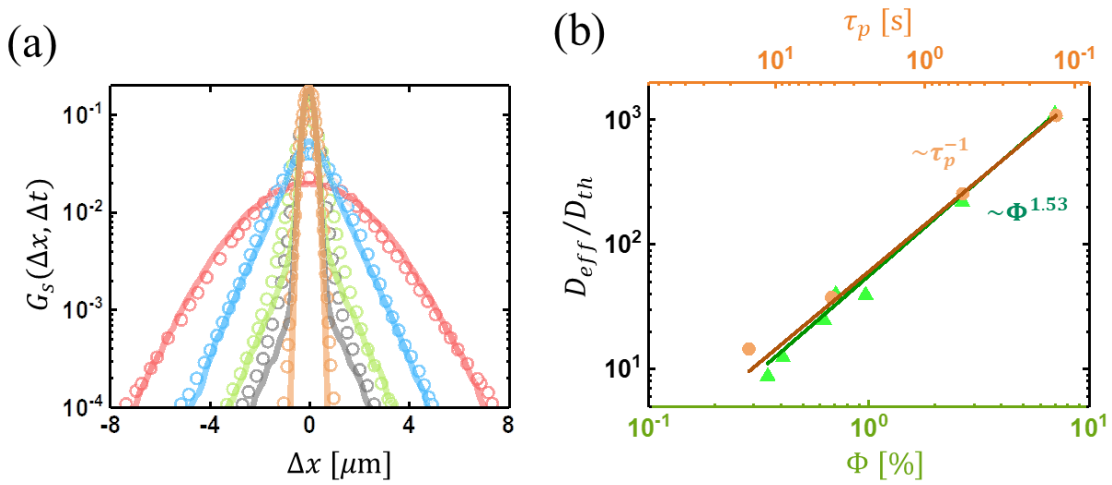

Figure 18: Simulation data of active noise model vs. the experimental data of the 1μm polystyrene beads (tracer) suspended in the active bath (algal cell). (a) The van Hove self-correlation function a given time ($\Delta t = 0.04\,\mathrm{s}$) at various cell volume fractions: $\Phi = 0\%$ (orange), 0.3% (gray), 0.7% (green), 2.7% (blue) and $\Phi = 7.0\%$ (red). The hollow circles represent the experimental data and the splines represents simulation results. Here, $\tau_p = 0.13\,\mathrm{s}$ (red), $\tau_p = 0.56\,\mathrm{s}$ (blue), $\tau_p = 4.2\,\mathrm{s}$ (green) and $\tau_p = 15\,\mathrm{s}$ (gray) at fixed $\tau_c = 0.3\,\mathrm{s}$ and $f_{RMS} = 0.4\,p\mathrm{N}$. (b) The normalized diffusion enhancement, defined as effective diffusion coefficient D_{eff} divided by thermal diffusion coefficient D_{th}. It is plot as a function of experimental volume fractions Φ (bottom axis), and simulated kick intervals τ_p (top axis). The experimental points (triangles) are fitted with $D_{eff} \sim \Phi^{1.53}$ and the simulation points (circles) are fitted with $D_{eff} \sim \tau_p^{-1}$.

4.4 Heat dissipation in an active bath.

4.4.1 Violation of Fluctuation-dissipation theorem in active bath

We study the energy (heat) dissipation in an active bath using our active force model. In this model, energy is continuously supplied to the tracer particles by the kick of the active particles in the active bath and the tracer particle dissipates the same amount of energy into the thermal bath in steady-state.[42] In this situation, the energy balance can be obtained by multiplying $\dot{x}$ to to Eq. (1).

$$\gamma \dot{x}\dot{x} = -\nabla V\left(x,\lambda(t)\right)\dot{x} + \xi_{th}(t)\dot{x} + \xi_{ext}(t)\dot{x} \tag{58}$$

Here, ξ_{ext} is the external force, V is the potential of particle, and $\lambda(t)$ is the parameter that controls the potential in time. Considering the chain rule of derivative in Eq. (58) as $dV\left(x,\lambda(t)\right) = \nabla V \cdot dx + \frac{\partial V}{\partial t}dt$.

$$\frac{dE}{dt} = \frac{\partial V}{\partial \lambda}\dot{\lambda} + \xi_{ext}(t)\dot{x} - \left[\gamma \dot{x} - \xi_{th}(t)\right]\dot{x} \tag{59}$$

Here, E represents the system energy and is equal to V in the overdamped case. According to the first law of thermodynamics, the energy rate of the tracer particle is $dE/dt = \dot{W} - \dot{Q}$. Here, the work rate of the tracer particle can be from two sources: one from the change of potential during the infinitesimal time dt and the other from the external force as $\dot{W} = \frac{\partial V}{\partial \lambda}\dot{\lambda} + \xi_{ext}(t)\dot{x}$. The heat dissipation rate is a kind of work done by the tracer particle on the thermal environment upon the change of the position $dx(t)$ during the infinitesimal time dt as $\dot{Q} = \left[\gamma \dot{x} - \xi_{th}(t)\right]\dot{x}$. When the system is in an equilibrium state (the potential does not change in time and there is no external force), $\langle dE/dt \rangle = \langle \dot{W} \rangle = \langle \dot{Q} \rangle = 0$ is satisfied. Therefore, the Fluctuation-Dissipation Theorem (FDT) is valid in the equilibrium condition as $C(t) = 2k_B T R(t)$. Here, $C(t)$ is the velocity auto-correlation function and $R(t)$ is the response function of the system.

However, FDT is not working in non-equilibrium conditions. Even though the energy of the system does not change in time in a non-equilibrium steady state, there is work that the tracer particle receives. Therefore, the following relationship is satisfied in a non-equilibrium steady state.[43, 44]

$$\left\langle \frac{dE}{dt} \right\rangle = 0, \quad \text{and } \langle \dot{W} \rangle = \langle \dot{Q} \rangle \geq 0 \tag{60}$$

Quantifying the heat dissipation and the work produced by the real bio-active particles is very important, but very difficult to do in the experiment. Especially in the overdamped system, we can not measure the particle velocity $\dot{x}(t)$ with time in Eq. (59).

Harada and Sasa[45] showed how to quantify the heat dissipation rate in the non-equilibrium conditions, known as the Fluctuation-Response Relation (FRR) which can be derived from Eq. (59).

$$\left\langle \dot{Q} \right\rangle = \gamma \left\{ v_s^2 + \int_{-\infty}^{\infty} \frac{d\omega}{2\pi} \left[C(\omega) - 2k_B T R(\omega) \right] \right\} \tag{61}$$

Here, v_s is the steady velocity of the system, $C(\omega)$ is the velocity auto-correlation function, and $R(\omega)$ is the response function of the system in the frequency domain.

4.4.2 Power spectral density of position

Figure 19 shows the power spectral density of position in the experiment with various conditions. These results agree with Eq. (21)

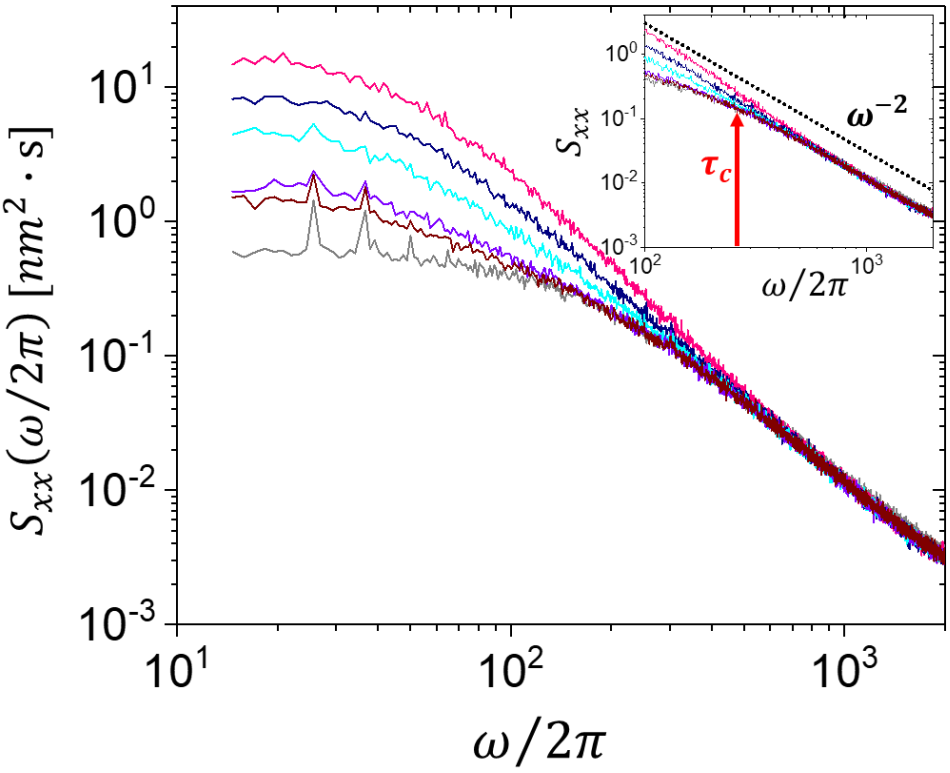

Figure 19: Power spectral density (PSD) of the particle position for various conditions; τ_p : $1ms$ (pink), $2ms$ (navy), $4ms$ (cyan), $12ms$ (purple), and $16ms$ (brown). Gray solid spline corresponds to PSD without the active force. Here, $X = 37nm$, $\tau_c = 4ms$, and $\tau_k = 1.1ms$. The inset is the magnified data near at the frequency corresponding to the time τ_c. Here, the black dotted line indicates the slope for free diffusion.

4.4.3 Velocity autocorrelation function $C(\omega)$

The velocity autocorrelation function is simply calculated from the power spectral density function in the overdamped case as,

$$\begin{aligned} C(\omega) &= v(\omega)v^*(\omega) = \omega^2 x(\omega)x^*(\omega) \\ &= \omega^2 S_{xx}(\omega) \end{aligned} \tag{62}$$

Here, $v(\omega)$ is the velocity in the frequency ω domain. Then, we can calculate the velocity autocorrelation using Eq. (21) and Eq. (62) as

$$C(\omega) = \frac{2\dfrac{\omega^2}{\tau_k}}{\omega^2 + \left(\dfrac{1}{\tau_k}\right)^2}\left[\frac{k_B T}{k} + \frac{k_B T}{k}\cdot\left(1+\frac{\tau_c}{\tau_k}\right)\cdot\left(\frac{1}{1+\omega^2\tau_c^2}\right)\right]. \tag{63}$$

4.4.4 Response function of the system $R(\omega)$

To obtain the response function $R(\omega)$, an infinitesimal perturbation $f^p(t)$ is applied to the system. In this case, the Langevin equation is written by

$$\gamma\dot{x}(t) = -kx(t) + \xi_{th}(t) + \xi_{act}(t) + f^p(t). \tag{64}$$

The general solution of Eq. (64) is $x(t) = \gamma^{-1}\int_0^t dt' \mathrm{e}^{-(t-t')/\tau_k}\left(\xi_{th}(t') + \xi_{act}(t') + f^p(t')\right)$, where the initial memory term $x(0)\mathrm{e}^{-t/\tau_k}$ is neglected in a steady-state. The ensemble average of the velocity is $\langle v(t)\rangle = \frac{1}{\gamma}\left[f^p(t) - \frac{1}{\tau_k}\int_0^t dt' \mathrm{e}^{-(t-t')/\tau_k} f^p(t')\right]$ and the response function $\delta\langle v(t)\rangle / \delta f^p(t')$ is given as

$$\chi(t,t') = \frac{1}{\gamma}\left[\delta(t-t') - \frac{1}{\tau_k}\mathrm{e}^{-(t-t')/\tau_k}\theta(t-t')\right]. \tag{65}$$

Note that the response function is independent of the active force as well as the thermal force. Figure 20 (a) shows the active force and the perturbation force at the time $t = t_0$. Fig. 20 (b) shows that the presence of the active noise $\xi_{act}(t)$ on the system does not change the response time τ_k. In this experiment the response time is $\tau_k = 1.1\,ms$. In frequency space ω, the system response function $R(\omega)$ from Eq. (65) is expressed as

$$R(\omega)=\frac{1}{\gamma}\cdot\frac{\omega^2}{\omega^2+\left(\frac{1}{\tau_k}\right)^2}. \tag{66}$$

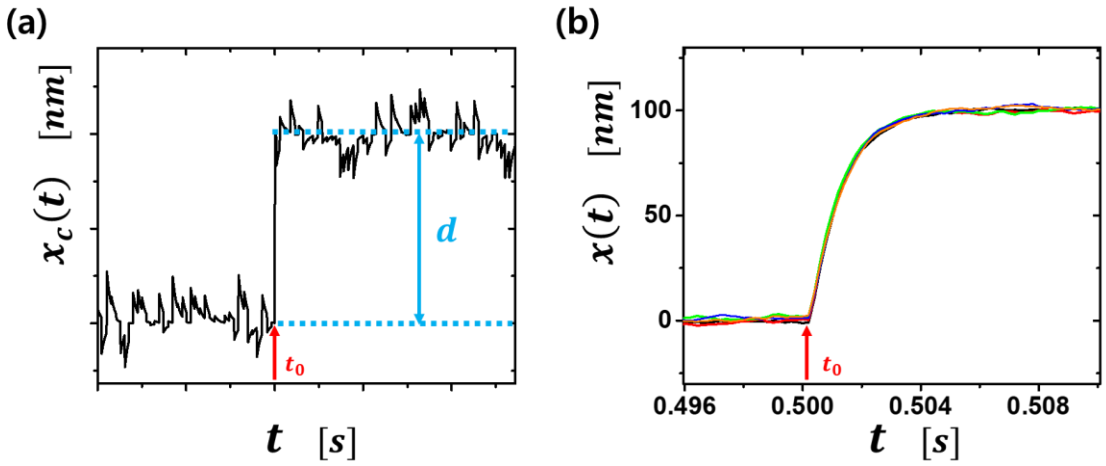

Figure 20: Measurement of the response function. (a) The center of the trap is instantly shifted with distance h at $t=t_0$. During this process, the system feels both the thermal and active fluctuations. (b) The trajectories of the tracer particle are averaged over 500 different measurements at the same condition. Different colors refer to different condition of active force.

4.4.5 Quantifying the heat dissipation rate

Form Eqs. (61), (63), and (66), we can calculate the amount of heat dissipation rate.

$$\left\langle \dot{Q} \right\rangle = \int_{-\infty}^{\infty} \frac{d\omega}{2\pi} D(\omega) \tag{67}$$

Here, $D(\omega) = \gamma\left[C(\omega) - 2k_B TR(\omega)\right]$. Figure 21 shows that the velocity autocorrelation function $C(\omega)$ (black solid line) and the response function $2k_B TR(\omega)$ [46] (purple dotted line) for various conditions. Fig. 21 (a) shows the data in an equilibrium condition. In this case the $C(\omega)$ and $2k_B TR(\omega)$ are the same, so FDT is valid. However, when the system is in non-equilibrium due to the presence of the active force, FDT is violated. Fig. 21 (b) shows that $C(\omega)$ becomes deviated from $2k_B TR(\omega)$ more as the active force increases. The response function does not change as long as the active force does not affect the intrinsic properties of the system.[47] Here, $D(\omega)$ represents the frequency ω dependent degree of violation of FDT, that is incidental to the heat dissipation rate. To quantify $\left\langle \dot{Q} \right\rangle$ using Eq. (63) and Eq. (66), we can obtain the analytical form of $D(\omega)$ as,

$$D(\omega) = \left(\frac{2k_B T_{act}}{\tau_c^2} \right) \cdot \left(1 + \frac{\tau_c}{\tau_p} \right) \cdot \left[\frac{\omega^2}{\left(\omega^2 + \frac{1}{\tau_k^2} \right)\left(\omega^2 + \frac{1}{\tau_c^2} \right)} \right]. \tag{68}$$

Using Eq. (67) and Eq. (68), we can obtain the analytical form of the energy dissipation rate.

$$\begin{aligned} \left\langle \dot{Q} \right\rangle &= 2\int_0^{\infty} \frac{d\omega}{2\pi} \left(\frac{2k_B T_{act}}{\tau_c^2} \right) \cdot \left(1 + \frac{\tau_c}{\tau_p} \right) \cdot \left[\frac{\omega^2}{\left(\omega^2 + \frac{1}{\tau_k^2} \right)\left(\omega^2 + \frac{1}{\tau_c^2} \right)} \right] \\ &= \frac{k_B T_{act}}{\tau_c}. \end{aligned} \tag{69}$$

Fig. 22 shows the average heat dissipation rate in various conditions. Here, the heat dissipation rate is proportional to the active temperature T_{act} and inversely proportional to the kick duration time τ_c.

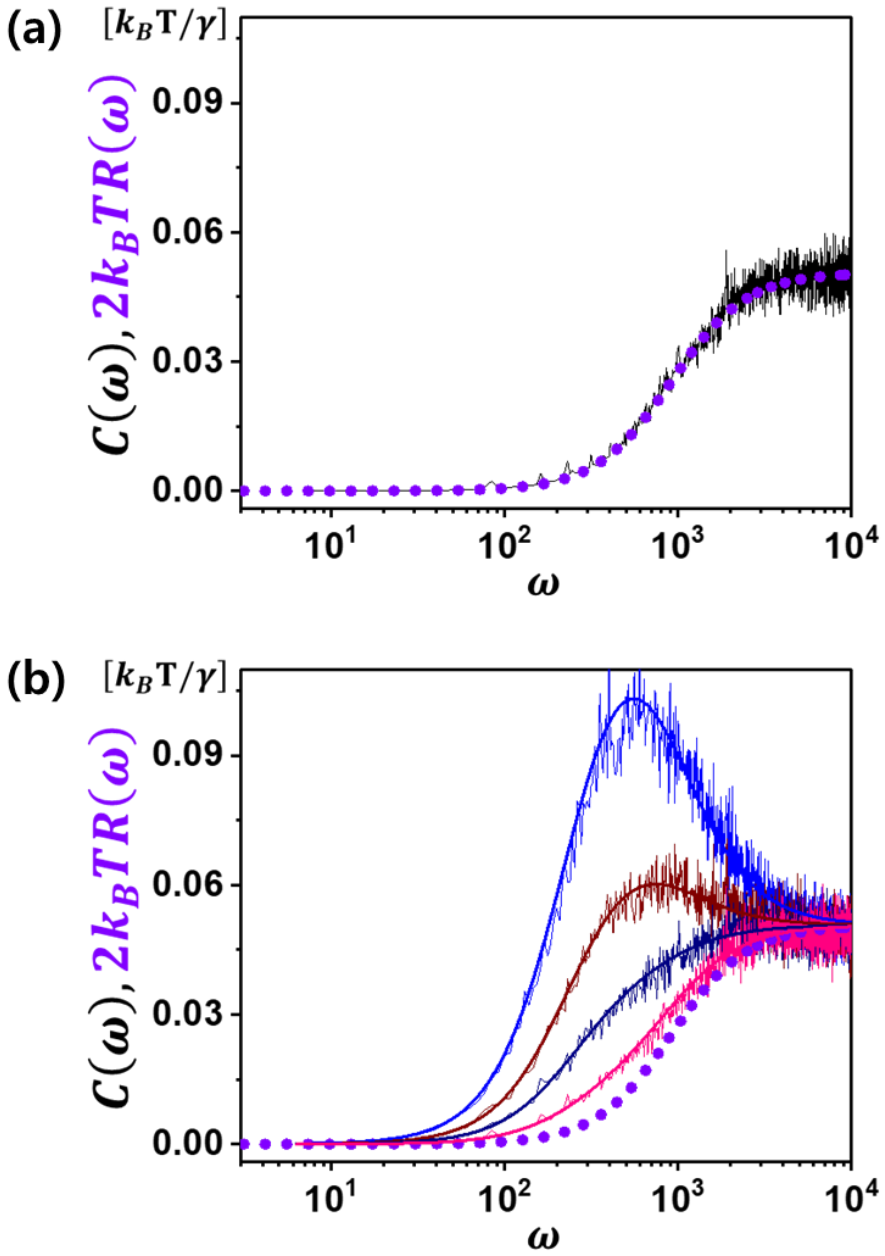

Figure 21: Measurement of the velocity autocorrelation and the response function of the tracer particle. (a) In an equilibrium condition, FDT is valid. Here, the experiment is carried out in the absence of active force. (b) In the non-equilibrium steady state, FDT is violated. Here, $\tau_p = 1ms$ (blue), $2ms$ (brown), $4ms$ (navy), and $12ms$ (pink), with fixed parameters $X = 37$ nm , $\tau_c = 4$ ms and $\tau_k = 1.1$ ms.

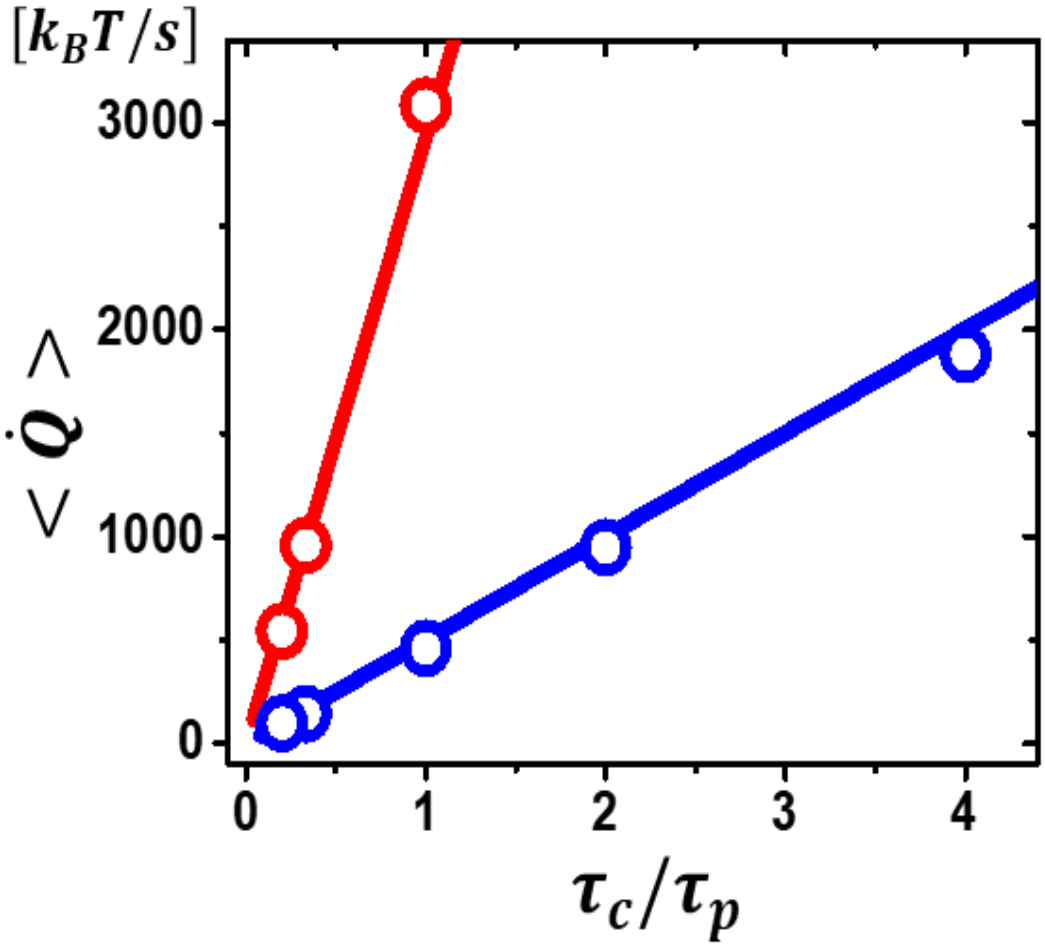

Figure 22: The total heat dissipation rate vs. τ_c/τ_p . Here, red (blue) color corresponds to $X = 70$ nm (37 nm) and $\tau_c = 2$ ms (4 ms). The solid lines are $\frac{k_B T_{act}}{\tau_c}$.

4.4.6 Quantifying the work production rate

The work production rate $\dot{W}$ can be defined in three different ways from Eq. (1) and (59). The first and second are to treat the random active force coming from the potential V without the external force $\xi_{ext}(t)$. The first one is from the viewpoint of the moving potential with center at $\xi_{act}(t)/k$. Therefore the energy balance is the following.

$$\begin{aligned}\frac{dE}{dt} &= \frac{\partial}{\partial t}\left[k\frac{\left(x-\xi_{act}(t)/k\right)^2}{2}\right]-\left[\gamma\dot{x}-\xi_{th}(t)\right]\dot{x} \\ &= -\left(x-\frac{\xi_{act}(t)}{k}\right)\dot{\xi}_{act}(t)-\left[\gamma\dot{x}-\xi_{th}(t)\right]\dot{x}\end{aligned} \tag{70}$$

Here, $V(t)=\frac{k}{2}\left(x-\xi_{act}(t)/k\right)^2$ and the work rate $\dot{W}$ is equal to $-\left(x-\xi_{act}(t)/k\right)\dot{\xi}_{act}(t)$. The second one is from the viewpoint that the particle feels both the fixed harmonic potential $kx^2/2$ and the active potential $x\xi_{act}(t)$.

$$\begin{aligned}\frac{dE}{dt} &= \frac{\partial}{\partial t}\left[\frac{kx^2}{2}-x\xi_{act}(t)\right]-\left[\gamma\dot{x}-\xi_{th}(t)\right]\dot{x} \\ &= -x\dot{\xi}_{act}(t)-\left[\gamma\dot{x}-\xi_{th}(t)\right]\dot{x}\end{aligned} \tag{71}$$

Here, $V(t)=kx^2/2-x\xi_{act}(t)$ and the work rate is expressed as $\dot{W}=-x\dot{\xi}_{act}(t)$. The third one is to treat the random active force as the external time-dependent force and the system feels only the time-independent harmonic potential. In this case, the Eq. (59) be expressed as

$$\begin{aligned}\frac{dE}{dt} &= \frac{\partial}{\partial t}\left[\frac{kx^2}{2}+x\xi_{act}(t)\right]-\left[\gamma\dot{x}-\xi_{th}(t)\right]\dot{x} \\ &= \xi_{act}(t)\dot{x}-\left[\gamma\dot{x}-\xi_{th}(t)\right]\dot{x}\end{aligned} \tag{72}$$

Here, $V=kx^2/2$ and the work rate is expressed as $\dot{W}=\xi_{act}(t)\dot{x}$. In all three cases, the heat dissipation rate $\dot{Q}$ has the same expression $\left(\gamma\dot{x}-\xi_{th}(t)\right)\circ\dot{x}$.

In the steady-state limit, all definitions of work rate lead to the same value as

$$\left\langle\dot{W}\right\rangle = k_B T_{act}/\tau_c = \left\langle\dot{Q}\right\rangle. \tag{73}$$

The work rate would have different value for each approach during the transient period. It can be calculated rigorously using the result in Section 5.3.

4.4.7 Maximum heat dissipation rate frequency

$D(\omega)$ is the spectral heat dissipation rate for a given frequency ω. Therefore, we can find the frequency of maximum heat dissipation rate ω_d by using $\partial D(\omega)/\partial\omega = 0$ and Eq. (68).

$$\left.\frac{\partial D(\omega)}{\partial \omega}\right|_{\omega=\omega_d} \equiv A\cdot\left[\frac{\partial}{\partial\omega}\left[\frac{\omega^2}{\left(\omega^2+\frac{1}{\tau_k^2}\right)\cdot\left(\omega^2+\frac{1}{\tau_c^2}\right)}\right]\right]_{\omega=\omega_d} = 0 \tag{74}$$

Here, $A = \left(\frac{2k_BT_{act}}{\tau_c^2}\right)\cdot\left(1+\frac{\tau_c}{\tau_p}\right)$.

$$\left.\frac{\partial D(\omega)}{\partial \omega}\right|_{\omega=\omega_d} = A\cdot\left[\frac{2\omega\left[\left(\omega^2+\frac{1}{\tau_k^2}\right)\cdot\left(\omega^2+\frac{1}{\tau_c^2}\right)\right]-\omega^2\left[4\omega^3+2\omega\left(\frac{1}{\tau_k^2}+\frac{1}{\tau_c^2}\right)\right]}{\left(\omega^2+\frac{1}{\tau_k^2}\right)^2\cdot\left(\omega^2+\frac{1}{\tau_c^2}\right)^2}\right]_{\omega=\omega_d} \tag{75}$$

$$\begin{aligned}&\Rightarrow 2\omega_d\left[\left(\omega_d^2+\frac{1}{\tau_k^2}\right)\cdot\left(\omega_d^2+\frac{1}{\tau_c^2}\right)\right]-\omega_d^2\left[4\omega_d^3+2\omega_d\left(\frac{1}{\tau_k^2}+\frac{1}{\tau_c^2}\right)\right]=0\\ &\Rightarrow \omega_d^4-\left(\frac{1}{\tau_c^2}\right)\left(\frac{1}{\tau_k^2}\right)=0\end{aligned} \tag{76}$$

Therefore, the maximum heat dissipation rate is found to be at the certain frequency, that is

$$\omega_d = \sqrt{\frac{1}{\tau_c\tau_k}}. \tag{77}$$

The time scale corresponding to this frequency is the geometric mean of τ_k and τ_c. During the equilibration time τ_k, the system relaxes dissipating energy. And during the kick duration time τ_c, the external energy is supplied. Therefore, it is not surprising that the time scale characterizing the maximum heat dissipation is the geometric mean of τ_k and τ_c. Figure 23 shows the spectral heat dissipation rate $D(\omega)$ from the experiment and the analytical prediction. They agree well with each other in various conditions.

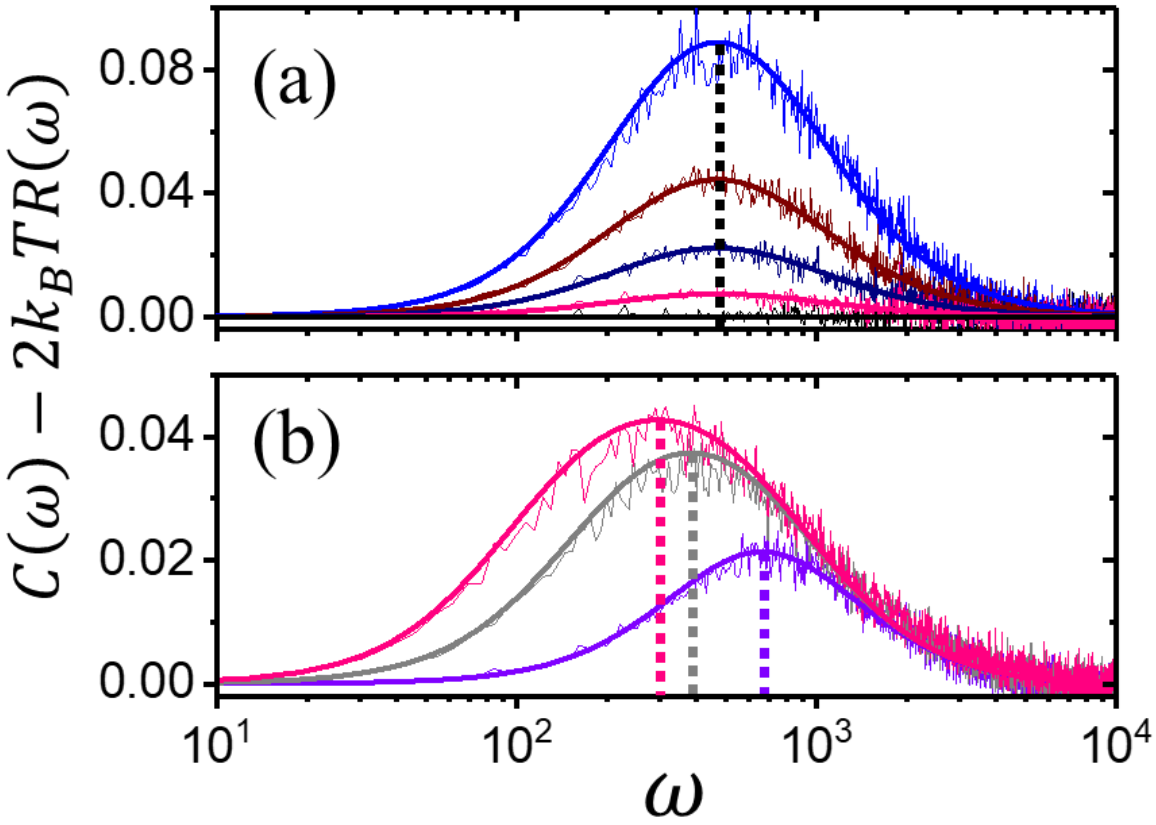

Figure 23: Semi-log graph of the spectral heat dissipation rate $D(\omega) = C(\omega) - 2k_BTR(\omega)$ vs. frequency ω for various conditions. The dotted line represents the maximum heat dissipation rate frequency. (a) Here $\tau_p = 1ms$ (blue), $2ms$ (brown), $4ms$ (navy), and $12ms$ (pink). The black solid line represents when there is no active force with fixed parameters $X = 37\,\text{nm}$, $\tau_c = 4\,\text{ms}$ and $\tau_k = 1.1\,\text{ms}$. (b) τ_c : $10ms$ (pink), $6ms$ (gray), and $2ms$ (purple) with fixed parameters $X = 70\,\text{nm}$, $\tau_p = 10\,\text{ms}$ and $\tau_k = 1.1\,\text{ms}$

V Appendix

5.1 **Simulation code (Matlab)**

```
%% parameters initialization
clc, clear, close all;
ns = 2500000;      % The number of sample
r = 1*10^-6 ;      % radius of the tracer particle [m]
kxx = 15.4;        % stiffness of real trap [pN/um]
xc = 70;           % strength length : 1st controlling parameter [nm]
tp = 3000;         % Possion interval time   : 2nd controlling parameter [nm]
tc = 600;          % active force duration :    3rd controlling parameter
sr2 = 2;           %Sampling rate    [realSR/sr2] [Hz]
nofs = 1000000;    % Number of data
kb = 1.38 * 10^-23;  % boltzman constant [J/K]
T = 297;           % Temperature [K]
eta = 0.93*10^-3;    % viscosity of water [N*s/m^2]

xxc = xc*10^-9 ;        % [m] change the unit
realSR = 20000;         % simulation physical time rate of simulation [Hz]
SR = 5000;              % observation time sampling rate [Hz]

kx = kxx * 10^-6; % [N/m]
deltaT = 1/SR;
realdeltaT = 1/realSR;
gamma = 6*pi*eta*r;              %
D = kb*T/gamma;                % Diffusiion coefficient  [m^2/s]
te = 1;
kk = 1;
nxc = zeros(ns,1);
noise = poissrnd(tp,1,1);
poissionset(kk) = noise;
Normali = sqrt(2*D*realdeltaT);     % normalization factor
nx(1,1) = 0;                    % initial position of particle
ndeltaTx = kx*realdeltaT/gamma;
fx = zeros(ns,1);
```

```
fx(1,1) = sqrt(1)*randn(1);

% generate the random Poisson interval time
for j = 2:ns
   if te == noise && noise ~=0
      nxc(j)=1;
      noise = poissrnd(tp,1,1);
      kk = kk+1;
      poissionset(kk) = noise;
      te = 0;
   elseif noise == 0
      nxc(j)=1;
      noise = poissrnd(tp,1,1);
      kk = kk+1;
      poissionset(kk) = noise;
   else
      nxc(j) = 0;
      te = te+1;
   end
end

nxcv = 0;
aa = 1;
for j = 2:ns
  if nxc(j) == 1;
     nxc(j) = nxc(j-1)*(exp(-1/tc))+sqrt(1)*randn(1)*xxc/Normali;
     nxcv = nxc(j);
     aa = 1;
  elseif nxc(j) == 0;
     nxc(j) = nxcv*(exp(-1*aa/tc));
     aa = aa+1;
  end
end
h = 1;
nxx = zeros(nofs,1);
nxx(1) = nx(1);
```

```
nxcs = zeros(nofs,1);

%% Run Langevin simulation
for j = 2:30000000
   nxcv = nxc(j);
   fx(j,1) = sqrt(1)*randn(1);          % Generate the random Gaussian (thermal noise)

   nx(j,1) = nx(j-1,1)*(1-ndeltaTy)+fx(j,1)+nxcv*ndeltaTx;  % normalized Langevin equation.
   if rem(j,sr2) == 0
      nxcs(h+1) = nxcv;
      nxx(h+1) = nx(j,1);
      h = h+1;
   end
   if h >= nofs
      break;
   end
end

%% simulation result
nor_x = nxx*Normali*10^9;       % tracer position data                x(t) [nm]
nor_nx = nxcs*Normali*10^9;     % center position of harmonic potential x_c(t) [nm]
```

5.2 The time-correlation function of active forces

The active force autocorrelation function using Eq. (4) can be expressed as

$$\begin{aligned}\left\langle \xi_{act}(t+\tau)\xi_{act}(t)\right\rangle &= k^2\left\langle\left[\sum_i^n d_i \mathrm{e}^{-(t+\tau-t_i)/\tau_c}\cdot\theta(t-t_i)\right]\left[\sum_j^n d_j \mathrm{e}^{-(t-t_j)/\tau_c}\cdot\theta(t-t_j)\right]\right\rangle \\ &= k^2\left(\left\langle\sum_{i=j}^n d_i^2 \mathrm{e}^{\frac{-2(t-t_i)+\tau}{\tau_c}}\right\rangle+\left\langle 2\sum_{i>j}^n d_i d_j \mathrm{e}^{\frac{-2t+t_i+t_j+\tau}{\tau_c}}\right\rangle\right).\end{aligned} \tag{78}$$

The second term $\langle\ldots\rangle$ on the right in Eq. (78) is zero, because of $\langle d_i d_j\rangle = X^2\delta_{ij}$. Then, Eq. (78) can be solved as

$$\begin{aligned}\left\langle k^2\sum_{i=j}^n d_i^2 \mathrm{e}^{\frac{-2(t-t_i)+\tau}{\tau_c}}\right\rangle &= \frac{1}{t}k^2\int_0^t\sum_{i=j}^n d_i^2 \mathrm{e}^{\frac{-2(t'-t_i)+\tau}{\tau_c}}dt' \\ &= \frac{\mathrm{e}^{\frac{-\tau}{\tau_c}}}{t}k^2\left[\int_{t_1}^t d_1^2 \mathrm{e}^{\frac{-2(t'-t_1)}{\tau_c}}dt'+\int_{t_2}^t d_2^2 \mathrm{e}^{\frac{-2(t'-t_2)}{\tau_c}}dt'+\cdots+\int_{t_n}^t d_n^2 \mathrm{e}^{\frac{-2(t'-t_n)}{\tau_c}}dt'\right] \\ &= \frac{\mathrm{e}^{\frac{-\tau}{\tau_c}}}{t}k^2\left[\frac{d_1^2}{2}\tau_c \mathrm{e}^{\frac{2t_i}{\tau_c}}\left(\mathrm{e}^{\frac{-2t_i}{\tau_c}}-\mathrm{e}^{\frac{-2t}{\tau_c}}\right)+\cdots+\frac{d_n^2}{2}\tau_c \mathrm{e}^{\frac{2t_n}{\tau_c}}\left(\mathrm{e}^{\frac{-2t_n}{\tau_c}}-\mathrm{e}^{\frac{-2t}{\tau_c}}\right)\right] \\ &= \frac{\mathrm{e}^{\frac{-\tau}{\tau_c}}}{t}k^2\left[\frac{d_1^2}{2}\tau_c+\frac{d_2^2}{2}\tau_c+\cdots+\frac{d_n^2}{2}\tau_c-\right. \\ &\qquad \left.\frac{d_1^2}{2}\tau_c \mathrm{e}^{\frac{-2(t-t_1)}{\tau_c}}-\frac{d_2^2}{2}\tau_c \mathrm{e}^{\frac{-2(t-t_2)}{\tau_c}}-\cdots-\frac{d_n^2}{2}\tau_c \mathrm{e}^{\frac{-2(t-t_n)}{\tau_c}}\right] \\ &= \frac{\mathrm{e}^{\frac{-\tau}{\tau_c}}}{t}k^2\left[\frac{\tau_c}{2}\sum_i^n d_i^2-\frac{\tau_c}{2}\sum_i^n d_i^2 \mathrm{e}^{\frac{-2(t-t_i)}{\tau_c}}\right].\end{aligned} \tag{79}$$

In the steady-state condition ($t >> \tau_c$), the active force autocorrelation function in Eq. (79) takes the following form

$$\begin{aligned}\lim_{t\to\infty}\left\langle \xi_{act}\left(t+\tau\right)\xi_{act}\left(t\right)\right\rangle &= \lim_{t\to\infty}k^2\frac{\mathrm{e}^{\frac{-\tau}{\tau_c}}}{t}\frac{\tau_c}{2}\sum_i^n d_i^2 \\ &= \lim_{t\to\infty}k^2\frac{\mathrm{e}^{\frac{-\tau}{\tau_c}}}{t}\frac{\tau_c}{2}nX^2 \\ &= \lim_{n\to\infty}k^2\frac{\mathrm{e}^{\frac{-\tau}{\tau_c}}}{n\tau_p}\frac{\tau_c}{2}nX^2 \\ &= \frac{1}{2}\frac{\left(kX\right)^2\tau_c}{\tau_p}\mathrm{e}^{\frac{-\tau}{\tau_c}}\end{aligned} \tag{80}$$

Here, n is the number of kick event during time t. Because of the Poisson property about the average kick interval time $\tau_p = \left\langle \Delta t_i \right\rangle = \frac{t}{n}$ as shown Fig. 3 (a), we used the n instead of time t in Eq. (80).

5.3 Work rate

5.3.1 Work rate (1)

The work rate is calculated by using Eq. (70) as follows.

$$\begin{aligned}\dot{W} &= \frac{\partial}{\partial t}\left[k\frac{\left(x-\xi_{act}(t)/k\right)^2}{2}\right] \\ &= -\left(x-\frac{\xi_{act}(t)}{k}\right)\dot{\xi}_{act}(t) \\ &= -\left(x_{th}+x_{act}-\frac{\xi_{act}(t)}{k}\right)\dot{\xi}_{act}(t)\end{aligned} \tag{81}$$

Here, we used the property $x = x_{th} + x_{act}$. By taking the ensemble average, we have

$$\left\langle \dot{W}\right\rangle = -\left\langle x_{act}\left(t\right)\dot{\xi}_{act}(t)\right\rangle + \frac{1}{k}\left\langle \xi_{act}(t)\dot{\xi}_{act}(t)\right\rangle, \tag{82}$$

Because the particle motion owing to the thermal noise is not correlated to the particle motion due to the active, $\left\langle x_{th}\left(t\right)\dot{\xi}_{act}(t)\right\rangle = 0$. First, the right hand first term in Eq. (82) is solved by using Eq. (6) as

$$\begin{aligned}\left\langle x_{act}\left(t\right)\dot{\xi}_{act}(t)\right\rangle &= \frac{1}{\gamma}\int_0^t dt' \mathrm{e}^{\frac{-k}{\gamma}(t-t')}\left\langle \xi_{act}\left(t'\right)\dot{\xi}_{act}\left(t\right)\right\rangle \\ &= \frac{1}{\gamma}\int_0^t dt' \mathrm{e}^{\frac{-k}{\gamma}(t-t')}\frac{d}{dt}\left\langle \xi_{act}\left(t\right)\xi_{act}\left(t'\right)\right\rangle \\ &= \frac{1}{\gamma}\int_0^t dt' \mathrm{e}^{\frac{-k}{\gamma}(t-t')}\frac{d}{dt}\left[\frac{k^2X^2\tau_c}{2\tau_p}\mathrm{e}^{\frac{-1}{\tau_c}(t-t')}\left(1-\mathrm{e}^{\frac{-2t'}{\tau_c}}\right)\right] \\ &= -\frac{k^2X^2}{2\gamma\tau_p}\int_0^t dt' \mathrm{e}^{\frac{-k}{\gamma}(t-t')}\mathrm{e}^{\frac{-1}{\tau_c}(t-t')}\left(1-\mathrm{e}^{\frac{-2t'}{\tau_c}}\right) \\ &= -\frac{k^2X^2}{2\gamma\tau_p}\mathrm{e}^{-\left(\frac{k}{\gamma}+\frac{1}{\tau_c}\right)t}\int_0^t dt'\left[\mathrm{e}^{\left(\frac{k}{\gamma}+\frac{1}{\tau_c}\right)t'}-\mathrm{e}^{\left(\frac{k}{\gamma}-\frac{1}{\tau_c}\right)t'}\right] \\ &= -\frac{k^2X^2}{2\gamma\tau_p}\mathrm{e}^{-\left(\frac{k}{\gamma}+\frac{1}{\tau_c}\right)t}\left\{\left(\frac{k}{\gamma}+\frac{1}{\tau_c}\right)^{-1}\left(\mathrm{e}^{\left(\frac{k}{\gamma}+\frac{1}{\tau_c}\right)t}-1\right)-\left(\frac{k}{\gamma}-\frac{1}{\tau_c}\right)^{-1}\left(\mathrm{e}^{\left(\frac{k}{\gamma}-\frac{1}{\tau_c}\right)t}-1\right)\right\}\end{aligned} \tag{83}$$

In steady-state condition ($t >> \tau_c$), Eq. (83) is simplified as

$$\begin{aligned}\left\langle x_{act}(t)\dot{\xi}_{act}(t)\right\rangle &= -\frac{k^2X^2}{2\gamma\tau_p}\left(\frac{k}{\gamma}+\frac{1}{\tau_c}\right)^{-1} \\ &= -\frac{kX^2\tau_c}{2\tau_p\tau_k}\left(\frac{1}{1+\frac{\tau_c}{\tau_k}}\right)\end{aligned} \tag{84}$$

In Eq. (82), the active force term is simply solved as

$$\begin{aligned}\left\langle \xi_{act}(t)\dot{\xi}_{act}(t)\right\rangle &= \frac{d}{dt}\left\langle {\xi_{act}}^2(t)\right\rangle \\ &= \frac{d}{dt}\left[\frac{k^2X^2\tau_c}{2\tau_p}\left(1-e^{\frac{-2t}{\tau_c}}\right)\right] \\ &= \frac{k^2X^2}{\tau_p}e^{\frac{-2t}{\tau_c}}.\end{aligned} \tag{85}$$

In steady-state condition ($t >> \tau_c$), Eq. (85) is zero. Therefore, the work rate is expressed as

$$\begin{aligned}\left\langle \dot{W}\right\rangle &= -\left\langle x_{act}(t)\dot{\xi}_{act}(t)\right\rangle + \frac{1}{k}\left\langle \xi_{act}(t)\dot{\xi}_{act}(t)\right\rangle \\ &= \frac{kX^2\tau_c}{2\tau_p\tau_k}\left(\frac{1}{1+\frac{\tau_c}{\tau_k}}\right) \\ &= \frac{k_BT_{act}}{\tau_c}\end{aligned} \tag{86}$$

5.3.2 Work rate (2)

The work rate is calculated by using Eq. (71) as follows.

$$\begin{aligned}\dot{W} &= \frac{\partial}{\partial t}\left[\frac{kx^2}{2}-x\xi_{act}(t)\right] \\ &= -x\dot{\xi}_{act}(t)\end{aligned} \tag{87}$$

By taking the ensemble average and using Eq. (84), we have

$$\begin{aligned}\left\langle \dot{W} \right\rangle &= -\left\langle x(t)\dot{\xi}_{act}(t) \right\rangle = -\left\langle x_{act}(t)\dot{\xi}_{act}(t) \right\rangle \\ &= \frac{k_B T_{act}}{\tau_c}.\end{aligned} \tag{88}$$

5.3.3 Work rate (3)

The work rate is calculated by using Eq. (72) as follows.

$$\dot{W} = \xi_{act}(t)\dot{x}(t) \tag{89}$$

By taking the ensemble average, we have the average work rate becomes as follows.

$$\begin{aligned}\left\langle \dot{W} \right\rangle &= \left\langle \xi_{act}(t)\dot{x}(t) \right\rangle \\ &= \left\langle \frac{\xi_{act}(t)+\xi_{act}(t-dt)}{2} \cdot \frac{x(t)-x(t-dt)}{dt} \right\rangle \\ &= \left\langle \frac{\xi_{act}(t)+\xi_{act}(t-dt)}{2} \cdot \frac{x_{act}(t)-x_{act}(t-dt)}{dt} \right\rangle \\ &= \frac{1}{2dt}\left\langle \left(\xi_{act}(t)+\xi_{act}(t-dt)\right)\cdot\left(x_{act}(t)-x_{act}(t-dt)\right) \right\rangle.\end{aligned} \tag{90}$$

The terms in the second round bracket in the right side about active position (x_{act} …) in Eq. (90) is solved as

$$\begin{aligned}x_{act}(t)-x_{act}(t-dt) &= \frac{1}{\gamma}\int_0^t dt' e^{\frac{-k}{\gamma}(t-t')}\xi_{act}(t') - \frac{1}{\gamma}\int_0^{t-dt} dt' e^{\frac{-k}{\gamma}(t-dt-t')}\xi_{act}(t') \\ &= \frac{1}{\gamma}\int_0^t dt' e^{\frac{-k}{\gamma}(t-t')}\xi_{act}(t') - \frac{1}{\gamma}\int_0^{t-dt} dt' e^{\frac{-k}{\gamma}(t-t')}\left(1+\frac{k}{\gamma}dt\right)\xi_{act}(t') \\ &= \frac{1}{\gamma}\left[\int_{t-dt}^t dt' \mathrm{e}^{\frac{-k}{\gamma}(t-t')}\xi_{act}(t') - \frac{k}{\gamma}dt\int_0^t dt' \mathrm{e}^{\frac{-k}{\gamma}(t-t')}\xi_{act}(t')\right].\end{aligned} \tag{91}$$

Therefore, the work rate is calculated as

$$\begin{aligned}\left\langle \dot{W} \right\rangle &= \frac{1}{2\gamma}\left[\frac{1}{dt}\int_{t-dt}^{t} dt' \mathrm{e}^{\frac{-k}{\gamma}(t-t')} \left(\left\langle \xi_{act}(t)\xi_{act}(t') \right\rangle + \left\langle \xi_{act}(t-dt)\xi_{act}(t') \right\rangle \right) \right. \\ &\qquad \left. -\frac{k}{\gamma}\int_{0}^{t} dt' \mathrm{e}^{\frac{-k}{\gamma}(t-t')} \left(\left\langle \xi_{act}(t)\xi_{act}(t') \right\rangle + \left\langle \xi_{act}(t-dt)\xi_{act}(t') \right\rangle \right) \right] \\ &\simeq \frac{1}{2\gamma}\left[2\frac{dt}{dt}\left\langle \xi_{act}{}^{2}(t) \right\rangle - 2\frac{k}{\gamma}\int_{0}^{t} dt \mathrm{e}^{\frac{-k}{\gamma}(t-t')} \left\langle \xi_{act}(t)\xi_{act}(t') \right\rangle \right].\end{aligned} \tag{92}$$

Then, using the time correlation of active force in Eq. (6), Eq. (92) becomes simplified as

$$\begin{aligned}\left\langle \dot{W} \right\rangle &= \frac{1}{\gamma}\frac{k^2X^2\tau_c}{2\tau_p}\left(1-e^{\frac{-2t}{\tau_c}} \right) - \frac{k^3X^2}{\gamma^2}\frac{\tau_c}{2\tau_p}\int_{0}^{t} dt' \mathrm{e}^{\frac{-k}{\gamma}(t-t')-\frac{1}{\tau_c}(t-t')} \left(1-\mathrm{e}^{\frac{-2t'}{\tau_c}} \right) \\ &= \frac{\tau_c}{2\tau_p}\frac{kX^2}{\tau_k}\left(1-e^{\frac{-2t}{\tau_c}} \right) - \frac{k^3X^2}{\gamma^2}\frac{\tau_c}{2\tau_p}\mathrm{e}^{-\left(\frac{k}{\gamma}+\frac{1}{\tau_c}\right)t} \left[\left(\frac{k}{\gamma}+\frac{1}{\tau_c} \right)^{-1} \left(\mathrm{e}^{\left(\frac{k}{\gamma}+\frac{1}{\tau_c}\right)t} - 1 \right) \right. \\ &\qquad \left. -\left(\frac{k}{\gamma}-\frac{1}{\tau_c} \right)^{-1} \left(\mathrm{e}^{\left(\frac{k}{\gamma}-\frac{1}{\tau_c}\right)t} - 1 \right) \right] \\ &= \frac{\tau_c}{2\tau_p}\frac{kX^2}{\tau_k}\left(1-e^{\frac{-2t}{\tau_c}} \right) - \frac{\tau_c}{2\tau_p\tau_k}kX^2\mathrm{e}^{-\left(\frac{k}{\gamma}+\frac{1}{\tau_c}\right)t} \left[\left(1+\frac{\tau_k}{\tau_c} \right)^{-1} \left(1-\mathrm{e}^{-\left(\frac{k}{\gamma}+\frac{1}{\tau_c}\right)t} \right) \right. \\ &\qquad \left. -\left(1-\frac{\tau_k}{\tau_c} \right)^{-1} \left(e^{\frac{-2t}{\tau_c}} - \mathrm{e}^{-\left(\frac{k}{\gamma}+\frac{1}{\tau_c}\right)t} \right) \right]\end{aligned} \tag{93}$$

In steady-state condition ($t >> \tau_c$), Eq. (93) is expressed as

$$\begin{aligned}\left\langle \dot{W} \right\rangle &= \frac{kX^2\tau_c}{2\tau_p\tau_k}\left(\frac{1}{1+\frac{\tau_c}{\tau_k}} \right) \\ &= \frac{k_BT_{act}}{\tau_c}.\end{aligned} \tag{94}$$

VI Conclusions

In summary, we studied the non-equilibrium stochastic thermodynamic view of the active matter system. Since the active matter system is in a non-equilibrium state, it is not easy to study the system by the experimental method. To overcome this, we made a simple active force model, tested it experimentally with optical trapping technology, and conducted computer simulations based on the equation of motion in Eq. (1). Our model is determined by three parameters: the average time interval between kicks τ_p which is related to the concentration of active particle, the kick duration τ_c which is related to characteristic time of active particle, and the kick strength X which is related to the random kicking intensity. This active force model covers not only the Poisson colored noise but also the well-known Ornstein-Uhlenbeck noise.

In the experiment, a tracer particle is surrounded by the environment created by both the thermal and active baths. The presence of the active bath enhances the diffusion of the tracer particle. Besides, the probability density distribution of the particle position no longer Gaussian-like, except when the average time interval between kicks is much shorter than the kick duration time. To test the model in the real bio-active systems, we conducted a computer simulation with our model and compared it with one previously published experiment. The results from the computer simulation agree very well with the experimental results. We also studied the energy balance of the system in the non-equilibrium condition. Since it is difficult to measure the amount of energy flow directly, the heat dissipation rate was measured using the fluctuation-dissipation theorem and the fluctuation-response relation. We found that the heat dissipation rate in the experiment is proportional to the active temperature (activity) of the tracer particles and inversely proportional to the correlation time of the active particle in steady-state. Experimentally measured heat dissipation rate agrees with the work rate in the steady-state which we derived analytically. The maximum heat dissipation rate is found to be at the certain frequency, that depends on parameters. The time scale corresponding to this frequency is coupled to the equilibration time τ_k and the kick duration time τ_c. This is not surprising because the system relaxes dissipating energy during τ_k and the external energy is supplied during τ_c.

The study performed in our work can be applied as a stochastic dynamic simulator. It can be applied for Brownian objects in different types of active baths in both cases of the computer simulations and experimental measurements. It does not require mechanistic understanding. It owes the comprehensive framework of rapid and simple prototyping protocol. However, the systems that work exhibit non-Gaussian behavior at equilibrium, has not been considered here. Different models are proposed in the literature to describe such behavior - "strange kinetics",[48] "diffusing diffusivity",[49] continuous-time random walks,[50] phenomenologies,[5, 51] and much more. In common, those situations share complexity not addressed here. First, these environments do not consist of simple harmonic potential as we posit

here. Second, even at the equilibrium, the noise is not necessarily Gaussian. While these features could, in principle, be addressed using the active model introduced here, to do so goes beyond the scope of the present study.

References

1. Wu, X. L.; Libchaber, A., Particle diffusion in a quasi-two-dimensional bacterial bath. *Phys Rev Lett* **2000,** *84* (13), 3017-20.

2. Goldstein, R. E.; Polin, M.; Tuval, I., Noise and synchronization in pairs of beating eukaryotic flagella. *Phys Rev Lett* **2009,** *103* (16), 168103.

3. Kurtuldu, H.; Guasto, J. S.; Johnson, K. A.; Gollub, J. P., Enhancement of biomixing by swimming algal cells in two-dimensional films. *Proc Natl Acad Sci U S A* **2011,** *108* (26), 10391-5.

4. Bechinger, C.; Di Leonardo, R.; Löwen, H.; Reichhardt, C.; Volpe, G.; Volpe, G., Active Particles in Complex and Crowded Environments. *Reviews of Modern Physics* **2016,** *88* (4).

5. Wang, B.; Anthony, S. M.; Bae, S. C.; Granick, S., Anomalous yet Brownian. *Proc Natl Acad Sci U S A* **2009,** *106* (36), 15160-4.

6. Dabelow, L.; Bo, S.; Eichhorn, R., Irreversibility in Active Matter Systems: Fluctuation Theorem and Mutual Information. *Physical Review X* **2019,** *9* (2).

7. Krishnamurthy, S.; Ghosh, S.; Chatterji, D.; Ganapathy, R.; Sood, A. K., A micrometre-sized heat engine operating between bacterial reservoirs. *Nature Physics* **2016,** *12* (12), 1134-1138.

8. Miño, G. L.; Dunstan, J.; Rousselet, A.; Clément, E.; Soto, R., Induced diffusion of tracers in a bacterial suspension: theory and experiments. *Journal of Fluid Mechanics* **2013,** *729*, 423-444.

9. Kummel, F.; Shabestari, P.; Lozano, C.; Volpe, G.; Bechinger, C., Formation, compression and surface melting of colloidal clusters by active particles. *Soft Matter* **2015,** *11* (31), 6187-91.

10. Yan, J.; Han, M.; Zhang, J.; Xu, C.; Luijten, E.; Granick, S., Reconfiguring active particles by electrostatic imbalance. *Nat Mater* **2016,** *15* (10), 1095-9.

11. Schmidt, F.; Liebchen, B.; Lowen, H.; Volpe, G., Light-controlled assembly of active colloidal molecules. *J Chem Phys* **2019,** *150* (9), 094905.

12. Jee, A. Y.; Dutta, S.; Cho, Y. K.; Tlusty, T.; Granick, S., Enzyme leaps fuel antichemotaxis. *Proc Natl Acad Sci U S A* **2018,** *115* (1), 14-18.

13. Jee, A. Y.; Cho, Y. K.; Granick, S.; Tlusty, T., Catalytic enzymes are active matter. *Proc Natl Acad Sci U S A* **2018,** *115* (46), E10812-E10821.

14. Gunther, J. P.; Majer, G.; Fischer, P., Absolute diffusion measurements of active enzyme solutions by NMR. *J Chem Phys* **2019,** *150* (12), 124201.

15. Wang, H.; Park, M.; Dong, R.; Kim, J.; Cho, Y. K.; Tlusty, T.; Granick, S., Boosted molecular mobility during common chemical reactions. *Science* **2020,** *369* (6503), 537-541.

16. Guo, M.; Ehrlicher, A. J.; Jensen, M. H.; Renz, M.; Moore, J. R.; Goldman, R. D.; Lippincott-Schwartz, J.; Mackintosh, F. C.; Weitz, D. A., Probing the stochastic, motor-driven properties of the cytoplasm using force spectrum microscopy. *Cell* **2014,** *158* (4), 822-832.

17. MacKintosh, F. C.; Levine, A. J., Nonequilibrium mechanics and dynamics of motor-activated gels. *Phys Rev Lett* **2008,** *100* (1), 018104.

18. Leptos, K. C.; Guasto, J. S.; Gollub, J. P.; Pesci, A. I.; Goldstein, R. E., Dynamics of enhanced tracer diffusion in suspensions of swimming eukaryotic microorganisms. *Phys Rev Lett* **2009,** *103* (19), 198103.

19. Purcell, E. M., Life at low Reynolds number. *American Journal of Physics* **1977,** *45* (1), 3-11.

20. Park, J. T.; Paneru, G.; Kwon, C.; Granick, S.; Pak, H. K., Rapid-prototyping a Brownian particle in an active bath. *Soft Matter* **2020,** *16* (35), 8122-8127.

21. Martínez, I. A.; Roldán, É.; Parrondo, J. M. R.; Petrov, D., Effective heating to several thousand kelvins of an optically trapped sphere in a liquid. *Physical Review E* **2013,** *87* (3).

22. Bérut, A.; Petrosyan, A.; Ciliberto, S., Energy flow between two hydrodynamically coupled particles kept at different effective temperatures. *EPL (Europhysics Letters)* **2014,** *107* (6).

23. Ashkin, A.; Dziedzic, J. M.; Bjorkholm, J. E.; Chu, S., Observation of a single-beam gradient force optical trap for dielectric particles. *Opt Lett* **1986,** *11* (5), 288.

24. Kanazawa, K., *STATISTICAL MECHANICS FOR ATHERMAL FLUCTUATION : non-gaussian noise in physics*. SPRINGER: [S.l.], 2018.

25. Fodor, É.; Hayakawa, H.; Tailleur, J.; van Wijland, F., Non-Gaussian noise without memory in active matter. *Physical Review E* **2018,** *98* (6).

26. Gomez-Solano, J. R.; Bellon, L.; Petrosyan, A.; Ciliberto, S., Steady-state fluctuation relations for systems driven by an external random force. *EPL (Europhysics Letters)* **2010,** *89* (6).

27. Van Kampen, N. G., Stochastic processes in physics and chemistry. **2007**.

28. Kanazawa, K.; Sano, T. G.; Sagawa, T.; Hayakawa, H., Minimal model of stochastic athermal systems: origin of non-Gaussian noise. *Phys Rev Lett* **2015,** *114* (9), 090601.

29. Paneru, G.; Dutta, S.; Sagawa, T.; Tlusty, T.; Pak, H. K., Efficiency fluctuations and noise induced refrigerator-to-heater transition in information engines. *Nat Commun* **2020,** *11* (1), 1012.

30. Paneru, G.; Lee, D. Y.; Tlusty, T.; Pak, H. K., Lossless Brownian Information Engine. *Phys Rev Lett* **2018,** *120* (2), 020601.

31. Maggi, C.; Paoluzzi, M.; Pellicciotta, N.; Lepore, A.; Angelani, L.; Di Leonardo, R., Generalized energy equipartition in harmonic oscillators driven by active baths. *Phys Rev Lett* **2014,** *113* (23), 238303.

32. Chaki, S.; Chakrabarti, R., Entropy production and work fluctuation relations for a single particle in active bath. *Physica A: Statistical Mechanics and its Applications* **2018,** *511*, 302-315.

33. Fodor, É.; Guo, M.; Gov, N. S.; Visco, P.; Weitz, D. A.; van Wijland, F., Activity-driven fluctuations in living cells. *EPL (Europhysics Letters)* **2015,** *110* (4).

34. Rahman, A., Correlations in the Motion of Atoms in Liquid Argon. *Physical Review* **1964,** *136* (2A), A405-A411.

35. He, X.; Wang, Y.; Tong, P., Dynamic heterogeneity and conditional statistics of non-Gaussian temperature fluctuations in turbulent thermal convection. *Physical Review Fluids* **2018,** *3* (5).

36. Kanazawa, K.; Sano, T. G.; Cairoli, A.; Baule, A., Loopy Levy flights enhance tracer diffusion in active suspensions. *Nature* **2020,** *579* (7799), 364-367.

37. Pince, E.; Velu, S. K.; Callegari, A.; Elahi, P.; Gigan, S.; Volpe, G.; Volpe, G., Disorder-mediated crowd control in an active matter system. *Nat Commun* **2016,** *7*, 10907.

38. Turiv, T.; Koizumi, R.; Thijssen, K.; Genkin, M. M.; Yu, H.; Peng, C.; Wei, Q.-H.; Yeomans, J. M.; Aranson, I. S.; Doostmohammadi, A.; Lavrentovich, O. D., Polar jets of swimming bacteria condensed by a patterned liquid crystal. *Nature Physics* **2020**.

39. Maggi, C.; Paoluzzi, M.; Angelani, L.; Di Leonardo, R., Memory-less response and violation of the fluctuation-dissipation theorem in colloids suspended in an active bath. *Sci Rep* **2017,** *7* (1), 17588.

40. Kurihara, T.; Aridome, M.; Ayade, H.; Zaid, I.; Mizuno, D., Non-Gaussian limit fluctuations in active swimmer suspensions. *Phys Rev E* **2017,** *95* (3-1), 030601.

41. Needleman, D.; Dogic, Z., Active matter at the interface between materials science and cell biology. *Nature Reviews Materials* **2017,** *2* (9).

42. Chaki, S.; Chakrabarti, R., Effects of active fluctuations on energetics of a colloidal particle: Superdiffusion, dissipation and entropy production. *Physica A: Statistical Mechanics and its Applications* **2019,** *530*.

43. Kubo, R., The fluctuation-dissipation theorem. *Reports on progress in physics* **1966,** *29* (1), 255.

44. Bellon, L.; Ciliberto, S.; Laroche, C., Violation of the fluctuation-dissipation relation during the formation of a colloidal glass. *Europhysics Letters (EPL)* **2001,** *53* (4), 511-517.

45. Harada, T.; Sasa, S., Equality connecting energy dissipation with a violation of the fluctuation-response relation. *Phys Rev Lett* **2005,** *95* (13), 130602.

46. Toyabe, S.; Jiang, H. R.; Nakamura, T.; Murayama, Y.; Sano, M., Experimental test of a new equality: measuring heat dissipation in an optically driven colloidal system. *Phys Rev E Stat Nonlin Soft Matter Phys* **2007,** *75* (1 Pt 1), 011122.

47. Dieterich, E.; Camunas-Soler, J.; Ribezzi-Crivellari, M.; Seifert, U.; Ritort, F., Single-molecule measurement of the effective temperature in non-equilibrium steady states. *Nature Physics* **2015,** *11* (11), 971-977.

48. Shlesinger, M. F.; Zaslavsky, G. M.; Klafter, J., Strange kinetics. *Nature* **1993,** *363* (6424), 31-37.

49. Chubynsky, M. V.; Slater, G. W., Diffusing diffusivity: a model for anomalous, yet Brownian, diffusion. *Phys Rev Lett* **2014,** *113* (9), 098302.

50. Schulz, J. H. P.; Chechkin, A. V.; Metzler, R., Correlated continuous time random walks: combining scale-invariance with long-range memory for spatial and temporal dynamics. *Journal of Physics A: Mathematical and Theoretical* **2013,** *46* (47).

51. Wang, B.; Kuo, J.; Bae, S. C.; Granick, S., When Brownian diffusion is not Gaussian. *Nat Mater* **2012,** *11* (6), 481-5.

Acknowledgement

Foremost, I want to thank my advisor Prof. Hyuk kyu Pak. He has given me continuous support for Ph.D study and research. He have impressed me, for bearance, inspiration, eagerness, and extensive knowledge. He was a great help for me in all my research time and writing this thesis. I can't imagine there would be a better supervisor than him.

Besides of my advisor, I appreciate my thesis committee members: Prof. Steve Granick, Prof. Yoon-Kyoung Cho, Prof. Joonwoo Jeong, and Prof. Chulan Kwon for their inspiration, percipient questions and comments.

My sincere gratitude goes to Dr. Govind Paneru and Dr. Kipom Kim for leading, helping, and enlightening me the first glance of research. I appreciate Dr. Chung-il Ha and Dr. Seong Jin Kim for encouragement and support. Also I thank Mr. Myung-Won song, Mr. Ki-Bom Nam, and Mr. Imran Saeed, who worked together as students in our group.

I thank my friends in IBS: Dr. Kisung Lee, for the research discussions, for helping me writing of this thesis. Mr. Myeonggon Park, Mr. Minju Kim, for all fun we have had during my Ph.D. Also I thank fellows in IBS: Yitan Li, Tian Hwang, Song Liu, and Kaikai Zheng, for the research discussions, for chatting, going hiking together. In particular, Dr. Ah Young Jee and Huan Wang, for giving me a lot of advices about life as well as about research. I am also grateful to the staffs: Ji Hee Hwang, Boram Kim, Bo Bae Shin, Seong Cheon Chu, Jae Kyoung Lee, and Su Jin Kim, for making the study comfortable.

And finally, thanks so much to my lovely family and friends.